Since January 2020 Elsevier has created a COVID-19 resource centre with free information in English and Mandarin on the novel coronavirus COVID-19. The COVID-19 resource centre is hosted on Elsevier Connect, the company's public news and information website.

Brain, Behavior, and Immunity 74 (2018) 186–204

Contents lists available at ScienceDirect

Brain, Behavior, and Immunity

journal homepage: www.elsevier.com/locate/ybrbi

Full-length Article

Microglia have a protective role in viral encephalitis-induced seizure development and hippocampal damage

Inken Waltl[a,b], Christopher Käufer[a], Ingo Gerhauser[c], Chintan Chhatbar[d], Luca Ghita[d], Ulrich Kalinke[b,d], Wolfgang Löscher[a,b,*]

[a] Department of Pharmacology, Toxicology, and Pharmacy, University of Veterinary Medicine Hannover, Germany
[b] Center for Systems Neuroscience, Hannover, Germany
[c] Department of Pathology, University of Veterinary Medicine Hannover, Germany
[d] Institute for Experimental Infection Research, TWINCORE, Center for Experimental and Clinical Infection Research, a Joint Venture Between the Helmholtz Center for Infection Research, Braunschweig, and the Hannover Medical School, Hannover, Germany

ARTICLE INFO

Keywords:
Seizures
Hippocampus
T cells
Monocytes
Spinal cord
Neuroinflammation

ABSTRACT

In the central nervous system (CNS), innate immune surveillance is mainly coordinated by microglia. These CNS resident myeloid cells are assumed to help orchestrate the immune response against infections of the brain. However, their specific role in this process and their interactions with CNS infiltrating immune cells, such as blood-borne monocytes and T cells are only incompletely understood. The recent development of PLX5622, a specific inhibitor of colony-stimulating factor 1 receptor that depletes microglia, allows studying the role of microglia in conditions of brain injury such as viral encephalitis, the most common form of brain infection. Here we used this inhibitor in a model of viral infection-induced epilepsy, in which C57BL/6 mice are infected by a picornavirus (Theiler's murine encephalomyelitis virus) and display seizures and hippocampal damage. Our results show that microglia are required early after infection to limit virus distribution and persistence, most likely by modulating T cell activation. Microglia depletion accelerated the occurrence of seizures, exacerbated hippocampal damage, and led to neurodegeneration in the spinal cord, which is normally not observed in this mouse strain. This study enhances our understanding of the role of microglia in viral encephalitis and adds to the concept of microglia-T cell crosstalk.

1. Introduction

Viral encephalitis is the most common form of brain infection and can cause severe and life-threatening consequences, including epilepsy (Vezzani et al., 2016). Monocyte infiltration and activation of microglia, the resident macrophage population of the brain, are hallmarks of CNS inflammation, including viral infection (Prinz and Priller, 2017). However, the role of these cells in viral clearance and immunopathology is not well defined. At least in part this is due to the problems of differentiating invading monocytes from activated microglia in the brain and the lack of selective tools to manipulate these two types of myeloid cells. In several viral brain infections, activated microglia appears to be involved in inhibition of viral replication and in neurotoxicity, indicating the dual nature of microglia: they contribute to the defense of the CNS but may also bear responsibility for CNS damage (Rock et al., 2004). Microglia expresses various Pattern Recognition Receptors (PRRs) to identify viral signatures called Pathogen Associated Molecular Patterns (PAMPs). Upon stimulation by PAMPs microglia respond by releasing several pro- and anti-inflammatory cytokines such as monocyte chemoattractant protein 1 (MCP1/CCL2), interleukin (IL)-1β, type I interferon (IFN), IFNγ, and tumor necrosis factor (TNF)α (O'Shea et al., 2013).

Recently, a new compound, PLX5622, which acts as specific dietary inhibitor of colony stimulating factor-1 receptor (CSF1R), a tyrosine kinase transmembrane receptor essential for the survival and activation of monocytes and macrophages in the periphery and microglia in the CNS (Erblich et al., 2011; Hamilton and Achuthan, 2013; Elmore et al., 2014), was shown to efficiently eliminate microglia in mice (Dagher et al., 2015). Similar to the less specific CSF1R inhibitor PLX3397 (Elmore et al., 2015), PLX5622 has been used to study the role of microglia in several conditions of brain injury (Acharya et al., 2016; Feng et al., 2016; Beckers et al., 2017; Hilla et al., 2017). Two recent studies

* Corresponding author at: Department of Pharmacology, Toxicology and Pharmacy, University of Veterinary Medicine, Bünteweg 17, D-30559 Hannover, Germany.
E-mail address: wolfgang.loescher@tiho-hannover.de (W. Löscher).

https://doi.org/10.1016/j.bbi.2018.09.006
Received 19 July 2018; Received in revised form 23 August 2018; Accepted 6 September 2018
Available online 11 September 2018
0889-1591/

reported that microglia depletion by PLX5622 increases virus replication and subsequent mortality in response to intracerebral infection with mouse hepatitis virus (MHV; Wheeler et al., 2018) or flaviviruses (West Nile virus and Japanese encephalitis virus; Seitz et al., 2018).

We used PLX5622 in a model of viral encephalitis in mice, in which Theiler's virus (also termed Theiler's murine encephalomyelitis virus [TMEV]), a naturally occurring enteric pathogen of the mouse, is used for intracerebral infection (Vezzani et al., 2016; DePaula-Silva et al., 2017). Disease development following TMEV infection depends on the mouse strain. The SJL/J mouse strain develops a multiple sclerosis-like progressive T cell-mediated autoimmune demyelinating disease, characterized by weakness of the hind limbs, which advances to a severe spastic paralysis, and inflammatory demyelination in the spinal cord, while the C57BL/6J (B6) mouse strain develops hippocampal damage and acute seizures, which progress to epilepsy (DePaula-Silva et al., 2017). The striking difference between the mouse strains seems to be partially due to the strong antiviral cytotoxic $CD8^+$ T lymphocyte response observed in B6 mice, which is suppressed by the elevated induction of regulatory $CD4^+$ T cells (Tregs) in SJL/J mice, resulting in viral persistence and demyelination (DePaula-Silva et al., 2017). We now report that elimination of microglia strikingly changes the disease phenotype of TMEV-infected B6 mice, indicating that microglia is much more important in this model of viral encephalitis than previously thought.

2. Materials and methods

2.1. Animals

Four-week-old female JAX® C57BL/6J (B6) mice were purchased from Charles River (Sulzfeld, Germany) and housed in groups under standardized conditions, 12 h/12 h day-night cycle, 50–60% humidity, 22–24 °C temperature and ad libitum tap water. Environmental enrichment was ensured by provision of housing and nesting material. Mice were randomly assigned into four experimental groups (vehicle vs. substance and subsequently into infected vs. mock-infected groups). According to a cooperative agreement between Charles River and The Jackson Laboratory, the JAX® C57BL/6J mouse strain bred by Charles River in Europe is genetically equivalent to that bred by The Jackson Laboratory in the U.S.

All animal experiments were conducted in accordance with the German Animal Welfare Law and were authorized by the local government (LAVES Oldenburg, Germany, permission number 33.9-42502-04-11/0516).

2.2. Treatment

Mice randomly assigned to the vehicle group received vehicle food chow, while mice randomly assigned to the treatment group had access to chow containing 1200 ppm PLX5622 per kilogram food chow (kindly provided by Plexxikon Inc., Berkeley, CA, USA). The regular food uptake of a 20–25 g mouse is 4 g per day, so the predicted overall intake of PLX5622 is 4.8 ppm per mouse per day. Treatment started 21 days prior to infection and continued until animals were sacrificed six to seven days post infection, resulting in a total treatment period of 28–29 days. This treatment protocol was established by Plexxikon and was previously used by other research groups (Dagher et al., 2015).

2.3. Infection

Intracerebral infection with the Daniels (DA) strain of TMEV was performed as previously described by Bröer et al. (2016, 2017) and Waltl et al. (2018). Therefore, a deep isoflurane inhalation anesthesia was induced and either 20 µl TMEV solution (2.44×10^7 PFU) or a mock solution were injected into the left parietal cortex of the mice using a free-hand method. The dose of TMEV was based on previous experiments of our group in B6 mice, to ensure a high incidence (> 50%) of early seizures in this mouse strain (Bröer et al., 2016).

2.4. Surveillance of body weight, seizures, and general behavior

Development of acute seizures, weight, general appearance and behavior in the first week after infection was assessed by animal monitoring twice daily for one hour, one h in the morning (between 9 and 12 a.m.) and one h in the afternoon (between 1 and 4 p.m.), with at least 3 h interval between the two recording sessions. Care was taken to avoid any group differences in recording periods by randomly assigning animals to the recording sessions. Recording was performed by experienced researchers, and the choice of recording periods was based on previous experiments with video-EEG monitoring of acute seizures in this model (for more details see Bröer et al., 2016, 2017).

2.5. Perfusion

On days 6 or 7 post infection animals were transcardially perfused with PBS followed by 4% paraformaldehyde. Brains and spleens were removed and left in formaldehyde overnight before being trimmed and embedded in paraffin. Additionally, segments of the spinal cord including the spinal column were removed, left in formaldehyde overnight, decalcified in EDTA for 48 h and afterwards embedded in paraffin. Animals used for flow cytometric analysis or RT-qPCR analysis were perfused with 4 °C PBS only. Brains for flow cytometry were harvested and stored in 4 °C PBS until being further processed, whereas brains for RT-qPCR were embedded in tissue freezing medium (Leica), frozen in liquid nitrogen and stored at −80 °C until further processing. For RT-qPCR analysis of the spinal cord, the spinal column was harvested, the vertebrae removed and the segments of the cord equally processed as brains for RT-qPCR analysis. EDTA-blood for flow cytometry was sampled prior to the start of perfusion analysis and stored at 4 °C.

2.6. Histology

Histological analyses of the brain were mainly focused on the dorsal hippocampus, as this brain structure is mainly damaged due to a hippocampal tropism of TMEV in B6 mice and is also associated with development of seizures and epilepsy (DePaula-Silva et al., 2017). Additionally, thalamic, hypothalamic and cortical regions were screened for morphological alterations and staining positivity. Furthermore, paraffin embedded sections of the cervical, thoracic and lumbal region of the spinal cord were examined to assess alterations in these regions.

Inflammatory processes were assessed by histological staining with H&E and additional immunohistochemistry staining with Mac-3 (Bio-Rad ABD Serotec GmbH, Puchheim, Germany), Iba1 (Wako Chemicals GmbH, Neuss, Germany and Abcam, Cambridge, GB), CD3 (DakoCytomation GmbH, Hamburg, Germany), Foxp3 (eBioscience; antibody-clone-FJK-16s-monoclonal/14-5773-80), TMEM119 (Abcam) and Iba1/Mac-3 fluorescent double staining and were analyzed as described recently (Bennett et al., 2016; Bröer et al., 2016; Ciurkiewicz et al., 2017; Waltl et al., 2018). H&E staining of spinal cord was used to examine neuronal necrosis, hypercellularity and perivascular infiltration and scored semi-quantitatively (Gerhauser et al., 2007). To assess the inflammatory signs in more detail, an additional Mac-3 staining was performed and scored semi-quantitatively (Bröer et al. 2016; Waltl et al., 2018) as follows: score: 0, absent (no positive, activated cells within the region); 1, mild (single positive cells found in the region); 2, moderate (up to 30% of region populated with positive cells); 3, severe (> 30% of region populated with positive cells). Data from both hemispheres were analyzed separately except for thalamus/hypothalamus and cerebral cortex, where Mac-3-positive cells were often in medial portions, so that these portions in both hemispheres were analyzed. CD3-positive, Foxp3-positive and TMEM119-positive cells within

the hippocampus and spinal cord were counted.

Neurodegeneration within the hippocampus was assessed using NeuN immunohistochemistry (Merck Millipore, Darmstadt, Germany) and scored semi-quantitatively (for details see Polascheck et al., 2010; Waltl et al., 2018). Also, Fluoro-Jade C (FJC) staining was performed to visualize the presence of degenerating neurons (Gröticke et al., 2008; Waltl et al., 2018). Glial fibrillary acid protein (GFAP) was immunostained to evaluate gliosis and astrocytosis in a semi-quantitative manner (Score: 0 = absent, 1 = mild, 2 = moderate, 3 = severe).

Virus antigen was stained using an anti-TMEV (VP1) antibody, and virus-positive cells within the brain were scored in a semi-quantitative manner (score 0, no stained cells; 1, few positively stained cells (< 10%); 2, 10–25% of cells stained; 3, > 25–45% of cells stained; 4, > 45% of cells stained), whereas virus-positive cells within the spinal cord were counted (Kummerfeld et al., 2009; Waltl et al., 2018). To assess demyelination within the spinal cord, Luxol-Fast-Blue staining was performed and slides were screened for signs of demyelination (Kummerfeld et al., 2009). To assess alterations of the myeloid system in the periphery, spleens were stained for Iba1 and TMEV and analyzed using the positive pixel count of the ImageJ software (Waltl et al., 2018).

All analyses were performed by two experienced researchers blinded to the experimental groups. Data of both researchers was averaged.

2.7. Immune cell isolation and flow cytometry

Immune cells were isolated from whole brain homogenates as recently described (Waltl et al., 2018). Briefly, in accordance to the manufacturer's specifications brain tissue was processed using the neural tissue dissociation kit (Miltenyi Biotec, Bergisch Gladbach, Germany). Afterwards, a percoll density gradient (30–37–70% percoll layers) was used for cell separation. Following density centrifugation, immune cells were washed and stained for 30 min at 4 °C using the following antibodies: CD11b APC-Cy7 (BD Biosciences; Heidelberg, Germany), and CD45.2 Pacific blue (Biolegend, San Diego, CA, USA). Respective isotype control antibodies or unstained samples were used to determine gates. A slightly adjusted protocol was used to isolate T-, and B-lymphocytes from whole brain homogenates. Therefore, the dissociation mix contained collagenase and DNAse and the following antibodies were used: CD45.2 Pacific blue, CD8ß PerCP-Cy5.5, Ly6C AF700, B220 PE-Cy5, CD4 FITC, CD44 brilliant violet 605, FoxP3 PE, Ly6G PE-Cy7, CCR2 AF647, MHCII PE (Biolegend, San Diego, CA, USA), and CD11c BV605 and CD11b APC-Cy7 (BD Biosciences; Heidelberg, Germany).

For flow cytometric analyses of blood samples, EDTA-blood was stained at 4 °C for 15 min with the following antibodies: B220 Pacific Blue, CD3 AF700 (Biolegend), CD11b APC-Cy7 (BD Biosciences), and CSF1R BV605 (Biolegend) (for more details see Waltl et al., 2018).

Flow cytometry was performed using a LSRII flow cytometer (BD Biosciences) and data was analyzed using FlowJo software (Tree Star, Ashland, OR, USA).

2.8. RT-qPCR

Ribonucleic acid (RNA) was isolated from frozen brain and spinal cord tissue using the RNeasy Lipid Tissue Mini Kit (Qiagen, Hilden, Germany) and subsequently transcribed into cDNA with the Omniscript RT Kit (Qiagen), Random Primers (Promega, Mannheim, Germany), and RNase Out (Invitrogen, Darmstadt, Germany). RT-qPCR was performed for TMEV, IL-1β, IL-6, IL-17, IL-34, Csf1r, TNFα, IFNγ, TGFβ1, and three housekeeping genes (GAPDH, β-Actin, HPRT) using standard protocols, the Mx3005P qPCR System (Agilent Technologies Deutschland GmbH, Böblingen, Germany), and Brilliant III Ultra-Fast SYBR®QPCR Master Mixes (Gerhauser et al., 2005, 2012). Forward (F) and reverse (R) primers designed for TMEV and murine genes were as follows: TMEV-F 5′-GACTAATCAGAGGAACGTCAGC-3′, TMEV-R 5′-GTGAAGAGCGGCAAGTGAGA-3′; IL-1β-F 5′-AGCTACCTGTGTCTTTCCCG-3′, IL-1β-R 5′-AGTGCAGTTGTCTAATGGGAAC-3′; IL-6-F 5′-GTTCTCTGGGAAATCGTGGA-3′, IL-6R 5′-CCAGAGGAAATTTTCAATAGGC-3′; IL-17-F 5′-ACTCTCCACCGCAATGAAGA-3′, IL-17R 5′-CTCTCAGGCTCCCTCTTCAG-3′; IL-34-F 5′-GCCACCTTTGCTGACCTAAG-3′, IL-34R 5′-TTTCCCAAAGCCACGTCAAG-3′; Csf1r-F 5′-AGGAGGTGACAGTGGTTGAG-3′, Csf1r-R 5′-CATGGTCTTGCACACGTAGG-3′; TNFα-F 5′-GCCTCTTCTCATTCCTGCTT-3′, TNFα-R 5′-CACTTGGTGGTTTGCTACGA-3′; IFNγ-F 5′-CACGGCACAGTCATTGAAAG-3′, IFNγ-R 5′-AATCTGGCTCTGCAGGATTT-3′; TGFβ1-F 5′-TTGCTTCAGCTCCACAGAGA-3′, TGFβ1-R 5′-TGGTTGTAGAGGGCAAGGAC-3′. Tenfold serial dilution standards ranging from 10^8 to 10^2 copies/µL were used to quantify the results. Experimental variations were corrected by using a normalization factor calculated from the housekeeping genes (Vandesompele et al., 2002). Melting curve analysis was performed to control the specificity of each reaction.

2.9. Statistics

GraphPad Prism Version 6 (La Jolla, CA, USA) was used for all statistical analyses. Depending on the distribution of the data, either parametric or nonparametric statistical tests were applied. For comparisons of two groups, either Student's *t*-test or Mann-Whitney *U* test were used; for more than two groups either one-way or two-way ANOVA for parametric or nonparametric data were used, followed by a post-hoc Dunnett's, Tukey's or Bonferroni's multiple comparisons test. The log-rank Mantel-Cox test was used for survival analysis. Seizure frequencies were compared using Fisher's exact test. A $P \leq 0.05$ was considered significant.

3. Results

Supplemental Table S1 gives an overview of the various experimental results of this study.

3.1. CSF1R inhibition depletes microglia in control and infected mice

Mice were treated with PLX5622, an orally bioavailable selective CSF1R inhibitor that crosses the blood–brain barrier (Dagher et al., 2015), for a period of 21 days prior to infection and treatment was continued until animals were killed 6–7 days after infection (Fig. 1). For this purpose PLX5622 was mixed into standard rodent chow at 1200 ppm.

To verify the microglia depletion, we used a microglia-selective antibody (TMEM119; Bennett et al., 2016). As shown in Fig. 2A for the hippocampus and para-hippocampal tissue, treatment with PLX5622 completely depleted microglia in mock-infected control mice and mice infected with TMEV, which was verified by counting TMEM119$^+$ cells in hippocampus (Fig. 2B). A similar lack of TMEM119-positive microglia was observed throughout the brain of PLX5622-treated mice. In infected B6 controls, significant microglia accumulation was seen in hippocampus and para-hippocampal regions (Fig. 2A and B).

We also quantitated CSF1R mRNA in the brain and spinal cord of mice with and without PLX5622, showing a significant increase in CSF1R upon infection in mice not treated with PLX5622 (Fig. 2C and D). In non-infected mice, expression of CSF1R was almost completely abolished by treatment with PLX5622, while a small but significant increase was seen in PLX5622-treated infected mice (Fig. 2D).

As described previously (Howe et al., 2012a; Cusick et al., 2013; Waltl et al., 2018), flow cytometry was used to differentiate CD45^{high} CD11b$^+$ cells, which are considered to be mainly brain-infiltrating blood-derived monocytes, from CD45^{low} CD11b$^+$ cells, which are considered to be mainly resident microglia, in the brain (Fig. 3A–D). Therefore, we will name these two cell populations monocytes and microglia in the following. We found that treatment with PLX5622

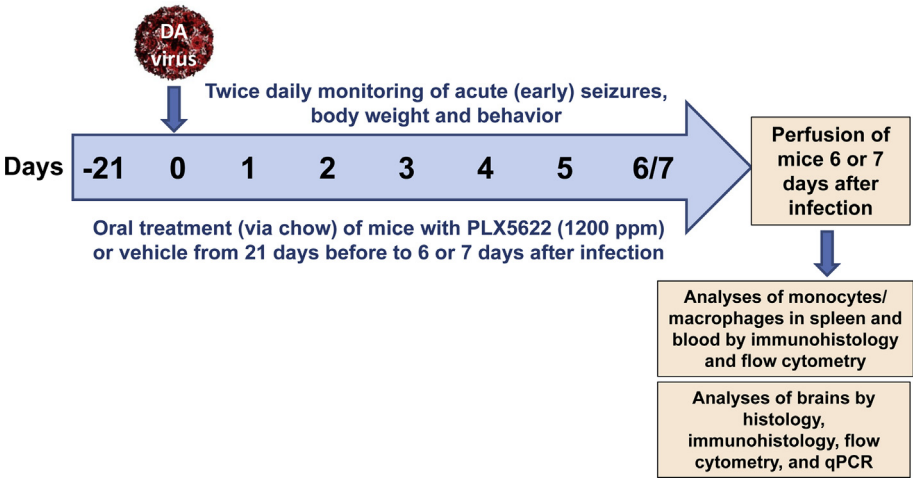

Fig. 1. Experimental protocol of the study. For details see the Methods section. Overall five experiments were performed with this protocol in groups of mice. First experiments were performed over 7 days following infection. However, the poor health status of the infected PLX5622 treated mice at day 7, resulting in mortality or euthanasia (see Results), led us shorten subsequent experiments to 6 days.

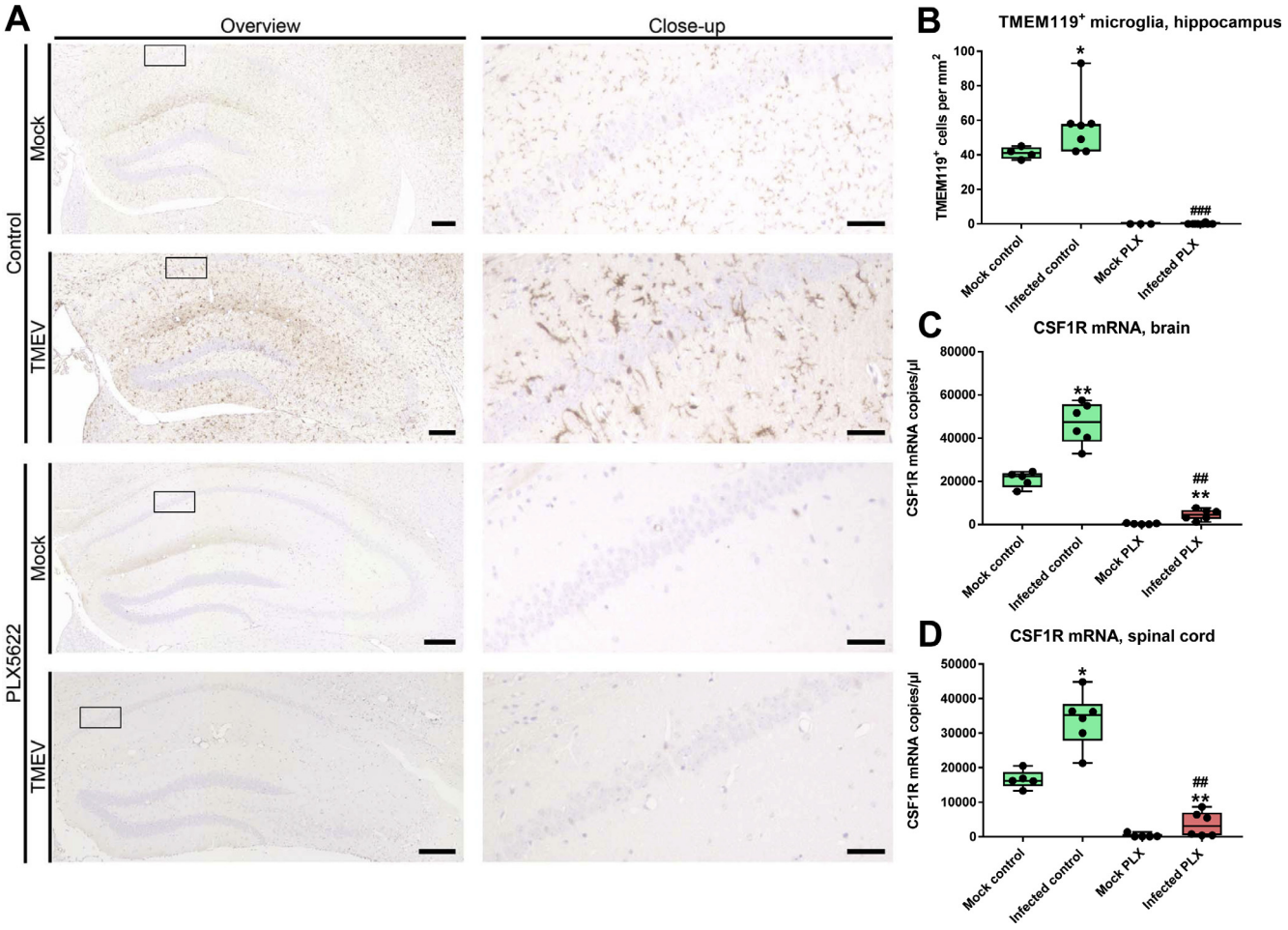

Fig. 2. Depletion of microglia via CSF1R inhibition by treatment with PLX5622 in Theiler's virus-infected mice. In the representative photomicrographs shown in A, microglia were immunostained with TMEM119. Infection increased TMEM119$^+$ cells in controls, which was completely inhibited by treatment with PLX5622. Quantification of data is shown in B (microglia in hippocampus). Data are shown as boxplots with whiskers from minimum to maximal values; the horizontal line in the boxes represents the median value. In addition, individual data are shown. Sample size: 4–5 mock-infected controls; 3–5 mock-infected mice with PLX5622; 6–7 infected controls; 6–8 infected mice with PLX5622. Significant differences to mock-infected mice are indicated by asterisks ($^*P < 0.05$; $^{**}P < 0.01$) while significant differences between infected mice treated with PLX5622 and infected controls are indicated by the hash sign ($^{\#}P < 0.05$; $^{\#\#}P < 0.01$; $^{\#\#\#}P < 0.001$). (B) TMEM119$^+$ cells in the hippocampus. Note the complete depletion of microglia in PLX5622-treated mice. (C) CSF1R mRNA quantitated by qPCR in the brains of mice. (D) CSF1R mRNA quantitated by RT-qPCR in the spinal cord of mice. All other details in C and D are as described above for B.

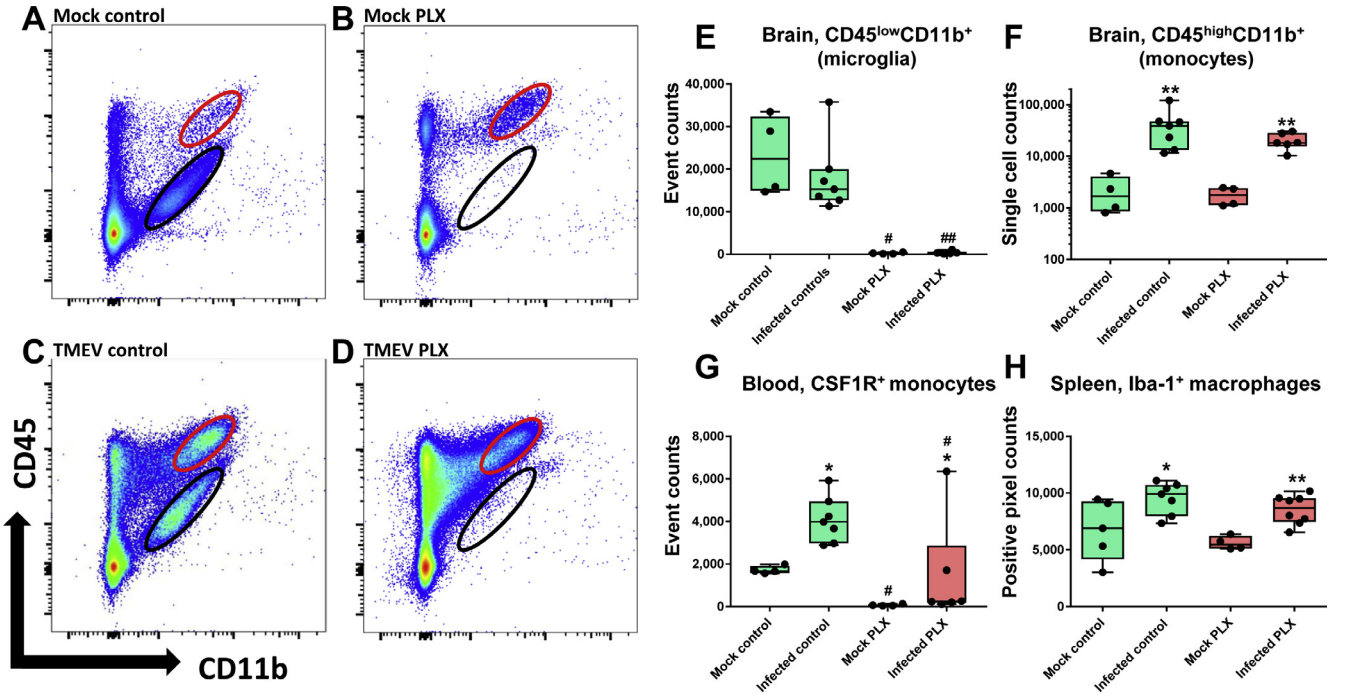

Fig. 3. Microglia and monocytes in Theiler's virus-infected mice. The figures in A-D present representative flow cytometry plots of brains from (A) a mock-infected control mouse, (B) a mock-infected control mouse that was treated with PLX5622, (C) a Theiler's virus (TMEV) infected mouse with vehicle treatment, (D) a Theiler's virus infected mouse treated with PLX5622. Animals were killed 6–7 days after infection as shown in Fig. 1. Microglia are indicated as $CD45^{low}$ $CD11b^{+}$ positive cells (black circle in each dot plot), while brain-infiltrating blood-derived monocytes are indicated as $CD45^{high}$ $CD11b^{+}$ cells (red circle in each dot plot). Note the scarcity of infiltrating macrophages in mock control (A) and the marked infiltration of such macrophages in the brain following virus infection (C, D). Also moderate microglia activation is seen in C, while treatment with PLX5622 almost completely depleted microglia in both mock-infected controls (B) and infected mice (D). Quantification of flow cytometric data is shown in E (microglia) and F (invading monocytes). Data are shown as boxplots with whiskers from minimum to maximal values; the horizontal line in the boxes represents the median value. In addition, individual data are shown. Sample size: 4–5 mock-infected controls; 4 mock-infected mice with PLX5622; 7 infected controls; 6–8 infected mice with PLX5622. Significant differences to mock-infected mice are indicated by asterisks ($^{*}P < 0.05$; $^{**}P < 0.01$) while significant differences between infected mice treated with PLX5622 and infected controls are indicated by the hash sign ($^{\#}P < 0.05$; $^{\#\#}P < 0.01$). (E) Microglia ($CD45^{low}$ $CD11b^{+}$) as analyzed by fluorescence-activated cell sorting. Note the complete depletion of microglia in PLX5622-treated groups. (F) Brain-infiltration of inflammatory monocytes ($CD45^{high}$ $CD11b^{+}$) as analyzed by fluorescence-activated cell sorting. Virus infection increased monocyte infiltration ~20 fold vs. mock, which was not affected by treatment with PLX5622. (G) Flow cytometric analysis of blood monocytes positive for colony stimulating factor 1 receptor ($CSF1R^{+}$) indicated significant increases by infection in both groups. (H) In the spleen, macrophages were immunostained by Iba1, demonstrating a significant increase in both infected groups. (For interpretation of the references to colour in this figure legend, the reader is referred to the web version of this article.)

almost completely depleted microglia in mock-infected control mice and mice infected with TMEV (Fig. 3B, D, E).

3.2. CSF1R inhibition does not affect monocyte invasion after infection

As shown in Fig. 3D and F, treatment with PLX5622 did not prevent the massive brain invasion of blood-derived monocytes after infection with TMEV. In the blood, infected mice exhibited a significant increase in $CSF1R^{+}$ monocytes, which was significantly reduced by PLX5622, but was still significantly higher than in mock-infected mice treated with PLX5622 (Fig. 3G). The number of $Iba1^{+}$ macrophages in spleen was not affected by treatment with PLX5622 (Fig. 3H).

3.3. CSF1R inhibition leads to an unfavorable ratio between regulatory T cells and effector T cells after infection

Next we examined whether treatment with PLX5622 affects the adaptive immune response to infection with TMEV. Infiltration of $CD3^{+}$ T-lymphocytes in the hippocampus was comparable in both groups (Fig. S1A). In addition, significant invasion of $CD4^{+}$ T lymphocytes ($CD4^{+}$ T effector cells) was observed in the brain of both infected groups, but $CD4^{+}$ cell invasion was significantly lower in the PLX5622-treated group (Fig. 4A). Significant brain invasion of $CD8^{+}$ cytotoxic T lymphocytes ($CD8^{+}$ T effector cells), which are thought to play a significant role in viral clearance in the TMEV model in mice (Libbey and Fujinami, 2011; DePaula-Silva et al., 2017), was observed both in infected controls and infected mice treated with PLX5622, without significant inter-group difference (Fig. 4B). The brain CD4:CD8 ratio was 0.34 in infected controls, demonstrating that brain invasion of $CD8^{+}$ T cells outnumbers invasion of $CD4^{+}$ T cells in this model. As a result of reduced $CD4^{+}$ T cell invasion in the PLX5622-treated group, the CD4:CD8 ratio was further reduced to 0.28. We also determined $CD4^{+}$ and $CD8^{+}$ cells in the spleen of infected mice (data not shown), resulting in a CD4:CD8 ratio of 1.3 in infected controls vs. 1.23 in PLX5622-treated animals.

Interestingly, in addition to the reduced invasion of $CD4^{+}$ T cells in the brain of microglia-depleted infected mice (Fig. 4A), the number of invading $CD4^{+}$ cells expressing the adhesion receptor CD44, which is upregulated after activation of naive T lymphocytes during their responses against viruses (Baaten et al., 2010), was significantly reduced in infected mice with depletion of microglia (Fig. 4C). The brain invasion of $Foxp3^{+}$ regulatory T cells (Tregs) was increased in both infected controls and PLX5622-treated infected mice to a similar extent without significant inter-group difference (Fig. 4D).

However, in the hippocampus, which is the main target of TMEV infection in B6 mice because of tropism of the virus to this region (Libbey and Fujinami, 2011), a significant invasion of $Foxp3^{+}$ Tregs was only observed in infected mice treated with PLX5622 (Fig. 4E). A

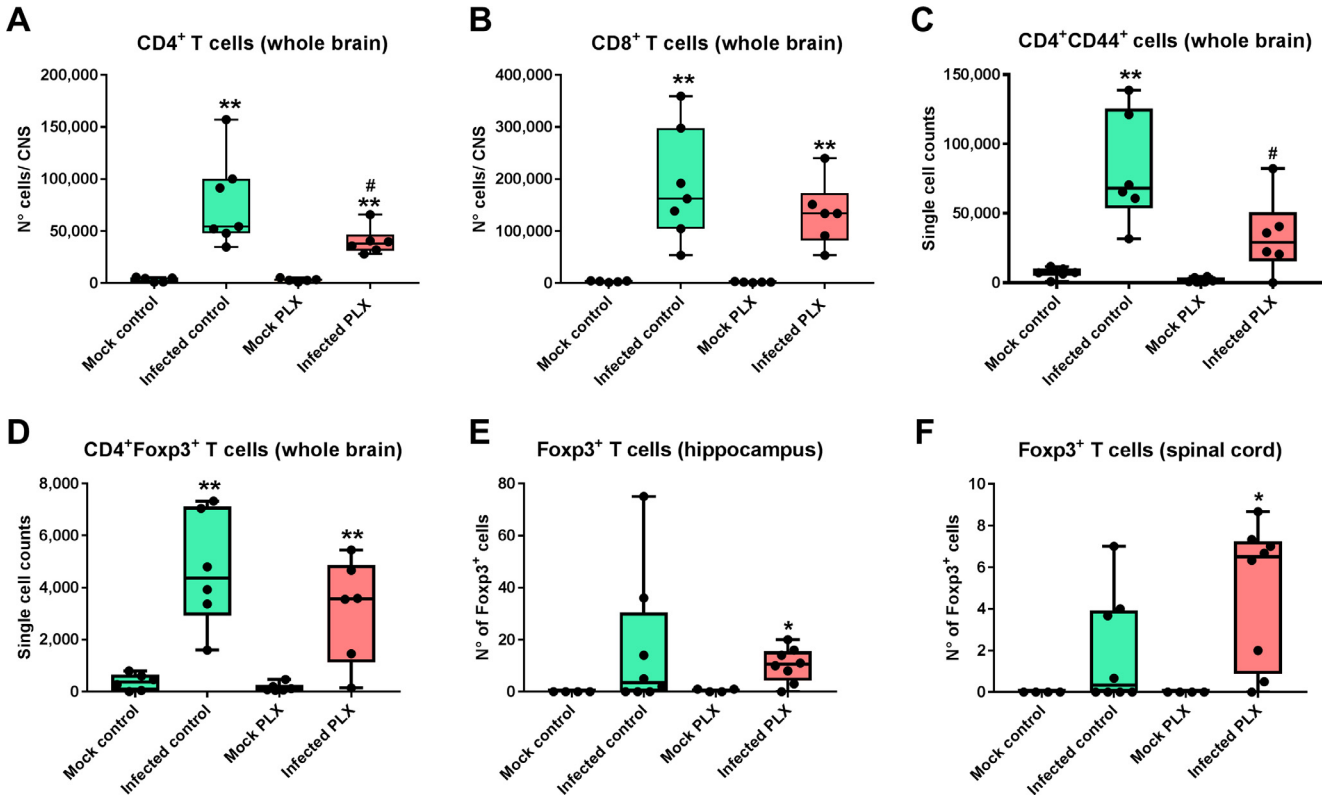

Fig. 4. Infiltration of T lymphocytes into the brain of Theiler's virus-infected mice. $CD4^+$ and $CD8^+$ T cells as well as $CD4^+CD44^+$ and $CD4^+Foxp3^+$ T cells were analyzed by flow cytometry using the whole brain; in addition, $Foxp3^+$ regulatory T cells (Tregs) were analyzed by immunohistochemistry in the hippocampus and spinal cord. Data are shown as boxplots with whiskers from minimum to maximal values; the horizontal line in the boxes represents the median value. In addition, individual data are shown. Sample size: 4–5 mock-infected controls; 5 mock-infected mice with PLX5622; 7–8 infected controls; 6–8 infected mice with PLX5622. Significant differences to mock-infected mice are indicated by asterisks ($^*P < 0.05$; $^{**}P < 0.01$) while significant differences between infected mice treated with PLX5622 and infected controls are indicated by the hash sign ($^{\#}P < 0.05$). (A) $CD4^+$ T lymphocytes were significantly increased in the brains of both infected groups, but the increase was significantly lower in PLX5622-treated mice. (B) $CD8^+$ T lymphocytes were significantly increased in the brains of both infected groups. (C) $CD4^+CD44^+$ cells were only increased in the brains of infected controls, but not the brains of microglia-depleted mice. (D) $CD4^+Foxp3^+$ cells were increased in the brains of both infected groups. (E) A significant increase in $Foxp3^+$ regulatory T cells in the hippocampus was only observed in infected PLX5622-treated mice. (F) In addition to the hippocampus shown in E, a significant increase in $Foxp3^+$ regulatory T cells was also observed in the spinal cord of infected PLX5622-treated mice.

similar finding was obtained for the spinal cord (Fig. 4F). Since $CD8^+$ T cell effector function is suppressed by elevated induction of Tregs (Richards et al., 2011), the significant increase in Tregs following CSF1R inhibition may lead to an unfavorable hippocampal and spinal cord ratio between Tregs and effector T cells, thus reducing antiviral immunity in these regions. This possibility is substantiated by the high increase in brain mRNA expression of the immunosupressive cytokine IL-10 in the brain of infected PLX5622-treated mice (see below), which is released by Tregs and suppresses the activation of cytotoxic T cells (O'Shea et al., 2013).

Compared to mock-infected controls, a modest but statistically significant brain infiltration of neutrophils was observed in infected controls. In the PLX5622-treated group only a trend ($P = 0.0826$) for neutrophil infiltration was observed, but both infected groups did not differ from each other (Fig. S1B).

3.4. Microglia depletion by CSF1R inhibition increases distribution and persistence of Theiler's virus in the brain

B6 mice typically survive the acute viral encephalitis and clear TMEV within 2 weeks after infection (Libbey and Fujinami, 2011). Furthermore, in this mouse strain the virus exhibits tropism to the CA1 and CA2 regions of the hippocampus following intracerebral infection (Libbey and Fujinami, 2011). As shown in Fig. 5A, C and D, in most B6 control mice Theiler's virus was already eliminated from the hippocampus by day 6/7, except for some staining in the CA2 in a few mice. In contrast, in mice treated with PLX5622, virus antigen was present throughout the hippocampus (Fig. 5B), resulting in significant increases in virus antigen-positive cells in the CA1/CA2 region of the hippocampus and other hippocampal regions (CA3, dentate gyrus) in which normally the virus is not present (Fig. 5C and D). At higher magnification, localization of the virus in neuronal cell bodies was visible in the hippocampus. In addition, virus antigen was infrequently observed outside neurons, associated with cells (most likely macrophages) around small vessels in the hippocampus. Furthermore, virus antigen was detectable in cerebral cortex, thalamus, hypothalamus (Fig. 5E), striatum and several other brain regions of PLX5622-treated mice, demonstrating that treatment with this compound increased the brain distribution of the virus. This is also illustrated by the presence of virus antigen in the spinal cord, in which the virus was not present in infected B6 vehicle controls (Fig. 5F). In addition to TMEV protein, we also determined TMEV mRNA, substantiating the significantly reduced elimination of the virus by treatment with PLX5622 (Fig. 5G and H).

3.5. CSF1R inhibition increases brain inflammation in the TMEV model

Immunohistochemistry with an antibody against Mac-3 was used to determine neuroinflammation in the hippocampus of infected mice. Mac-3 (also known as CD107b and LAMP-2) is a glycoprotein that is expressed at the plasma membrane of both activated microglia and

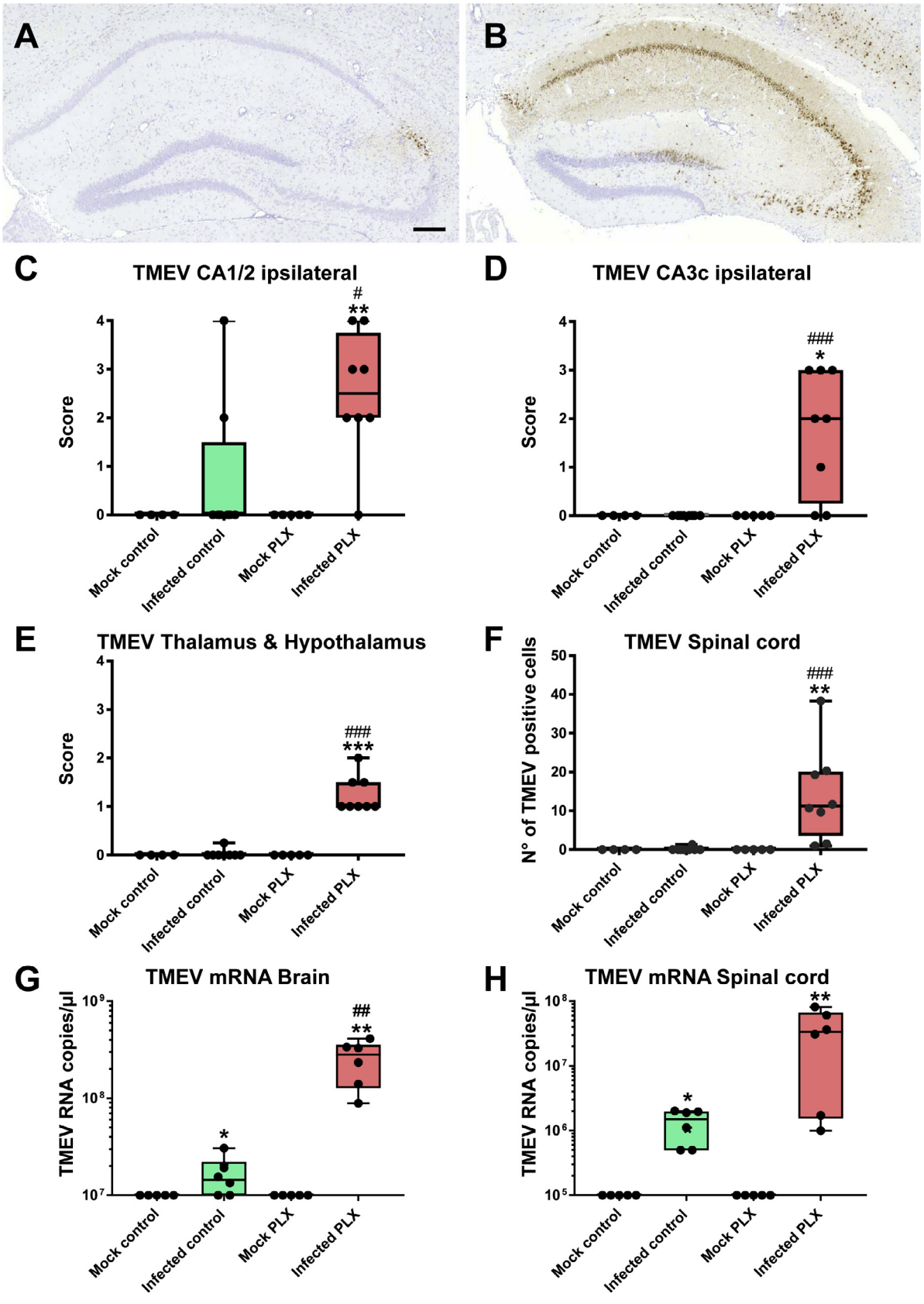

(caption on next page)

Fig. 5. Hippocampal distribution of Theiler's virus (TMEV) antigen. (A) A representative photomicrograph of an infected control mouse, demonstrating virus antigen only in the CA2 region. Scale bar in A = 200 μm. (B) A representative photomicrograph of an infected mouse with PLX5622 treatment, demonstrating virus antigen in all cell layers of the hippocampus. At higher magnification, localization of the virus in neuronal cell bodies was visible. (C–F) (Semi)quantitative data for antigen expression. Data are shown as boxplots with whiskers from minimum to maximal values; the horizontal line in the boxes represents the median value. In addition, individual data are shown. Sample size: 4 mock-infected controls; 5 mock-infected mice with PLX5622; 8 infected controls; 8 infected mice with PLX5622. Significant differences to mock-infected mice are indicated by asterisks ($^{*}P < 0.05$; $^{**}P < 0.01$; $^{***}P < 0.001$) while significant differences between infected mice treated with PLX5622 and infected controls are indicated by the hash sign ($^{\#}P < 0.05$; $^{\#\#}P < 0.01$; $^{\#\#\#}P < 0.001$). (C) Expression of TMEV antigen in the CA1/CA2 layers of the ipsilateral hippocampus. Treatment with PLX5622 significantly increased virus antigen expression in infected mice. (D) Expression of TMEV antigen in the CA3c layer of the ipsilateral hippocampus. Treatment with PLX5622 significantly increased virus antigen expression in infected mice. (E) Expression of TMEV antigen in the thalamus and hypothalamus. Treatment with PLX5622 significantly increased virus antigen expression in infected mice. (F) Expression of TMEV antigen in the spinal cord. Treatment with PLX5622 significantly increased virus antigen expression in infected mice. (G) Expression of TMEV mRNA in the brain. Treatment with PLX5622 significantly increased virus mRNA expression in infected mice. (H) Expression of TMEV mRNA in the spinal cord.

invading monocytes (Prinz et al., 2008). As shown in Fig. 6, at one week after infection, only some infected B6 control mice exhibited Mac-3$^+$ cells in the hippocampus, whereas significant increase in Mac-3$^+$ cells was observed in the cerebral cortex, thalamus and hypothalamus. Neuroinflammation was increased by treatment with PLX5622 in that significant increase in Mac-3$^+$ cells was also observed in hippocampal CA1, CA2, CA3, and dentate gyrus (Fig. 6). Mac-3 labeling in the contralateral hemisphere was similar to that in the ipsilateral hemisphere shown in Fig. 6.

For further evaluating the activation status of myeloid cells in the brain, the amount of Iba1- and Mac-3-immunolabeled cells was compared in the hippocampus. Ionized calcium binding adaptor molecule 1 (Iba1) is a calcium-binding protein that labels both resting and activated microglia and infiltrating monocytes, whereas Mac-3 labels only activated microglia and invading monocytes (Greter et al., 2015). Regarding Iba1-labeling, almost no such labeling was observed in mock-infected controls (Fig. 7A), while the number of Iba1$^+$ cells significantly increased in infected controls (Fig. 7B). In PLX5622-treated infected mice, the number of Iba1$^+$ cells was lower in the CA1/CA2 region compared to infected controls (Fig. 7D) but not in other hippocampal regions (CA3c shown as example in Fig. 7E). However, a difference in Iba1$^+$ cell shape was observed in that both round and ramified cells were observed in infected controls (Fig. 7B), representing monocytes and resting and activated microglia, whereas only round cells were observed in PLX5622-treated mice (Fig. 7C), substantiating the depletion of microglia as indicated by flow cytometry.

Depending on the hippocampal sub-region and treatment, on average 20–70% of the Iba1-labeled cells in infected mice were also positive for Mac-3. The number of Iba1/Mac-3 double labeled cells in the hippocampus did not significantly differ between infected controls and PLX5622-treated mice (Fig. 7F and G). However, when the activation percentage was calculated (i.e., the percentage of Iba1/Mac-3 double-labeled cells in percent of all Iba1-labeled cells), it was significantly higher in PLX5622-treated mice than infected controls in the CA3c (Fig. 7I) and perivascular area (data not shown).

For further characterizing the neuroinflammation following infection, we determined perivascular cuffing and hypercellularity in HE stained sections of the hippocampus. Perivascular cuffing, the accumulation of lymphocytes and monocytes in a dense mass around vessels, is a typical sign of viral encephalitis (Libbey and Fujinami, 2011). Similarly, hypercellularity, which results from disease-associated infiltration of lymphocytes and monocytes but also from astrocytosis and microgliosis, is an indicator of neuroinflammation. As shown in Suppl. Fig. S1C and D, infected B6 vehicle control mice only rarely exhibited perivascular infiltrates (PVI) at 1 week after infection, whereas a significant number of such infiltrates were observed in the hippocampus of PLX5622-treated mice. The same was true for hypercellularity (Supplemental Fig. S1E).

In addition to microglia, astrocytes are activated in response to TMEV infection in B6 mice, which can be labeled by glial fibrillary acidic protein (GFAP); GFAP$^+$ astrocytes are particularly prominent in the hippocampus of infected mice (Libbey and Fujinami, 2011). In the present experiments, the number of GFAP$^+$ astrocytes was only rarely different between mock-infected controls and TMEV-infected B6 control mice, whereas a marked astrogliosis was observed in PLX5622-treated mice (Supplemental Figs. S1F and S2). Within the hippocampus, GFAP$^+$ astrocytes were primarily located in the tissue adjacent to the damaged cell layers (Supplemental Fig. S2). Gliosis was also observed in the corpus striatum of all infected mice (not illustrated).

3.6. CSF1R inhibition increases neurodegeneration in the TMEV model

When neurons were stained by NeuN, the most marked neuronal damage in infected B6 vehicle controls was observed in the CA2 region of the hippocampus (Fig. 8A, E–H). Treatment with PLX5622 significantly increased neuronal damage in the hippocampus (Fig. 8B, E–H). Significant neuron loss was also observed in parahippocampal cortex (not illustrated).

For further analysis of neurodegeneration in the hippocampus and other brain regions, sections were stained with Fluoro-Jade C (FJC), a sensitive and specific fluorescent marker of dying neurons (Schmued et al., 2005). In mock-infected controls, no FJC-stained neurons were observed (not illustrated), while intense staining of pyramidal cells was observed in the CA1 and CA2 layers of some infected B6 vehicle controls (Fig. 8C). In infected mice treated with PLX5622, FJC-labeled neurons were not only observed in CA1 and CA2 but all regions of the hippocampal formation, including CA3, the granule cell layer of the dentate gyrus and the dentate hilus (Fig. 8D). Furthermore, FJC-labeled neurons were observed in the cortex. Counting of FJC-positive cells in the hippocampus substantiated the impression of visual inspections of sections in that infected mice treated with PLX5622 exhibited significantly more degenerating neurons in the hippocampus than infected controls (see Fig. 8I and J as examples; significant differences also observed in CA3a, CA3c, and dentate gyrus).

3.7. CSF1R inhibition induces inflammation and neurodegeneration in the spinal cord of infected mice

In contrast to SJL/J mice, B6 mice typically do not develop a chronic inflammatory demyelinating disease in the spinal cord, so B6 mice are considered to be resistant to the TMEV-induced demyelinating disease (Libbey and Fujinami, 2011). Consistent with this view, infected B6 control mice did not show any indication of cell death or inflammation in the spinal cord (Fig. 9C) except for a moderate increase in CD3$^+$ T lymphocytes and Mac-3 labeling (Fig. 9K and L). Furthermore, myelin staining did not reveal any demyelination (Fig. 9E). In contrast, PLX5622-treated mice exhibited TMEV antigen (Fig. 9A), necrosis of motor neurons (Fig. 9B and G) and inflammation in the spinal cord (Fig. 9D, H–J), thus explaining the paralysis observed in these mice (see below). Also, a significant increase in Foxp3$^+$ regulatory T cells was only observed in PLX-treated mice (Fig. 4D). Demyelination was not observed in PLX5622-treated mice (Fig. 9F), which may be due to the fact that mice were killed 6–7 days after infection, because demyelination is known to develop slowly in sensitive mouse strains such as SJL/J (DePaula-Silva et al., 2017).

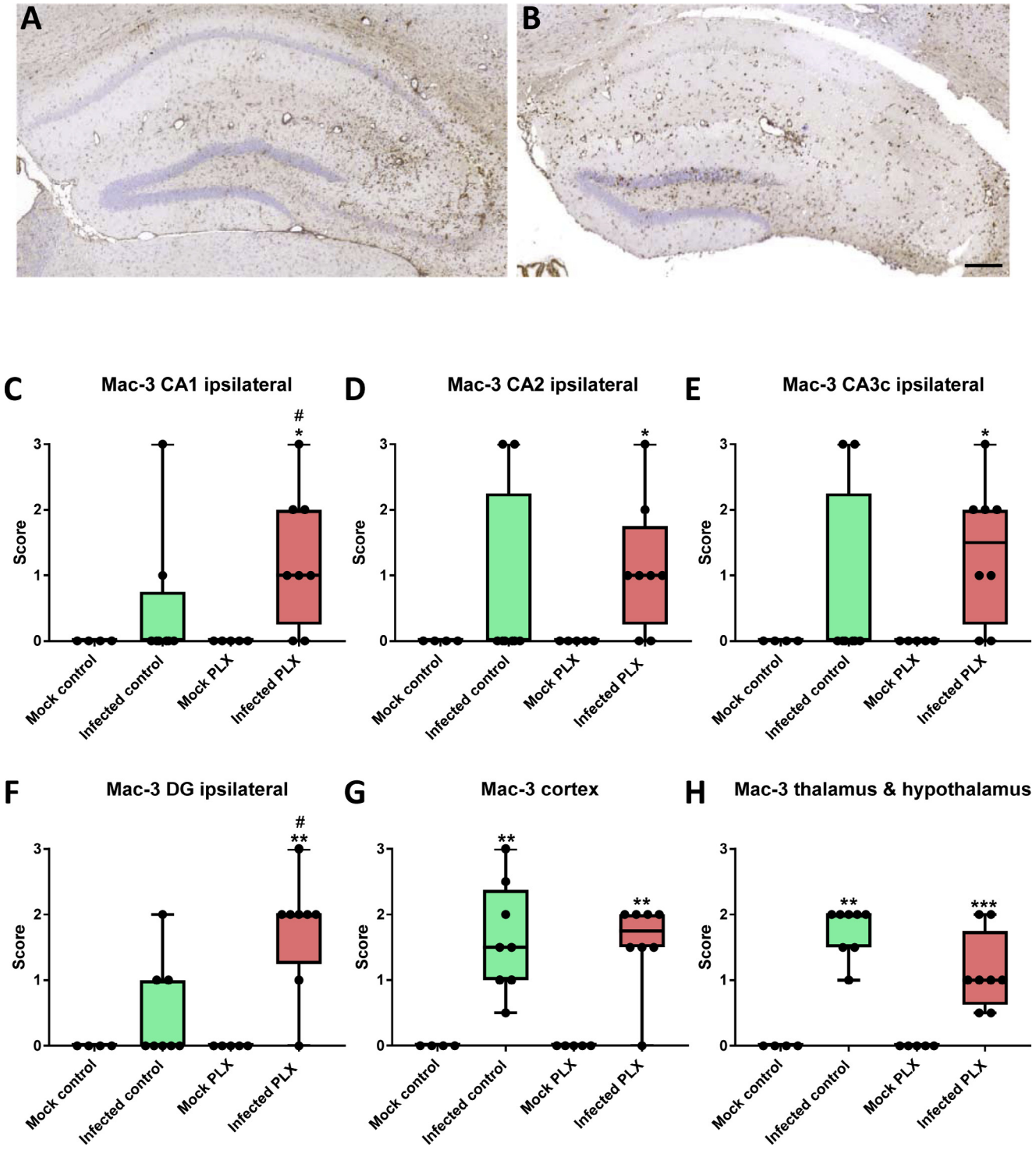

Fig. 6. Neuroinflammation as indicated by Mac-3 labeling of activated microglia and infiltrating monocytes in the brain of Theiler's virus-infected mice. (A) A representative photomicrograph of an infected control mouse. (B) A representative photomicrograph of an infected mouse with PLX5622 treatment. Scale bar in B = 200 μm. (C–H) Semiquantitative data for expression of Mac-3. Data are shown as boxplots with whiskers from minimum to maximal values; the horizontal line in the boxes represents the median value. In addition, individual data are shown. Sample size: 4 mock-infected controls; 5 mock-infected mice with PLX5622; 8 infected controls; 8 infected mice with PLX5622. Significant differences to mock-infected mice are indicated by asterisks ($^{*}P < 0.05$; $^{**}P < 0.01$; $^{***}P < 0.001$) while significant differences between infected mice treated with PLX5622 and infected controls are indicated by the hash sign ($^{\#}P < 0.05$). (C) Scores for Mac-3 labeling in the ipsilateral CA1 of the hippocampus. At the time chosen (6–7 days after infection), significant difference to mock controls is only observed for infected mice treated with PLX5622. (D) Scores for Mac-3 labeling in the ipsilateral CA2 of the hippocampus. Significant difference to mock controls is only observed for infected mice treated with PLX5622. (E) Scores for Mac-3 labeling in the ipsilateral CA3c of the hippocampus. Significant difference to mock controls is only observed for infected mice treated with PLX5622. (F) Scores for Mac-3 labeling in the ipsilateral dentate gyrus (DG) of the hippocampus. Significant difference to mock controls is only observed for infected mice treated with PLX5622. (G) Scores for Mac-3 labeling in the cerebral cortex. Significant difference to mock controls is observed for both infected groups. (H) Scores for Mac-3 labeling in the thalamus and hypothalamus. Significant difference to mock controls is observed for both infected groups.

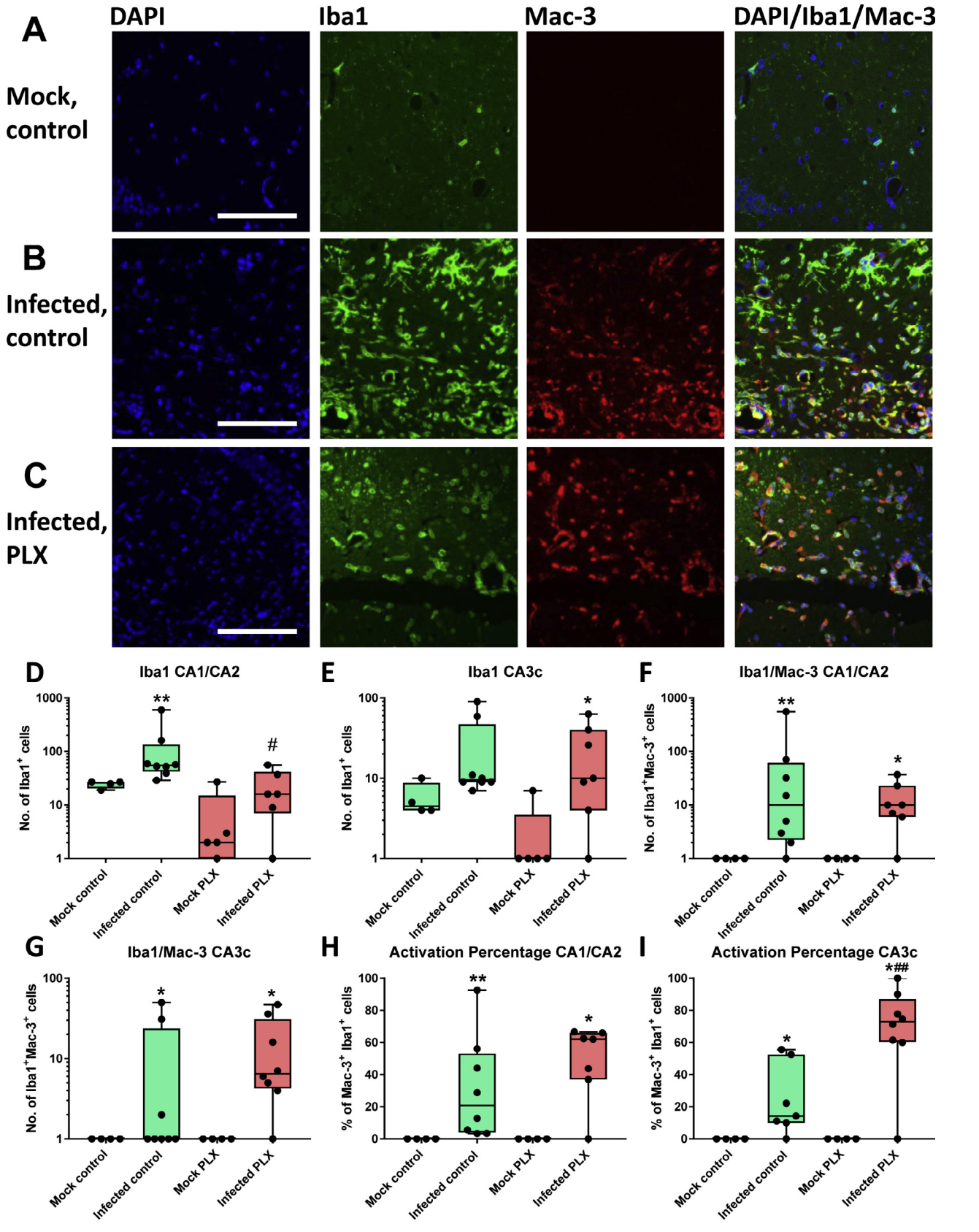

(caption on next page)

Fig. 7. Neuroinflammation as indicated by Iba1 and Mac-3 labeling and double labeling. While Iba1 labels both resting and activated microglia and infiltrated monocytes in the brain, Mac-3 only labels activated microglia and infiltrated monocytes. (A) Representative photomicrographs of a mock-infected control mouse. The first graph shows labeling of cell nuclei by DAPI in blue, the second graph Iba1 labeled cells in green, the third graph Mac-3 labeled cells in red, and the fourth graph cells labeled for both Iba1 and Mac-3. Only few Iba1 and no Mac-3 labeled cells are visible, consistent with the lack of neuroinflammation in mock-infected mice. (B) Representative photomicrographs of an infected control mouse. Note the marked increase in both Iba1 and Mac-3 labeling. Both ramified and round cell types are visible. Iba1 and Mac-3 double labeled cells are indicated in yellow. (C) Representative photomicrographs of an infected mouse with PLX5622 treatment. Note the lack of ramified cells, which is due to microglia depletion. Scale bar in A, B and C = 100 μm. (D–I) Quantitative data for expression of Iba1, Iba1/Mac-3 double labeled cells, and the "activation percentage" indicated by Iba1/Mac-3 double labeling. Data are shown as boxplots with whiskers from minimum to maximal values; the horizontal line in the boxes represents the median value. In addition, individual data are shown. Sample size: 4 mock-infected controls; 4–5 mock-infected mice with PLX5622; 7–8 infected controls; 6–8 infected mice with PLX5622. Significant differences to mock-infected mice are indicated by asterisks ($^{*}P < 0.05$; $^{**}P < 0.01$) while significant differences between infected mice treated with PLX5622 and infected controls are indicated by the hash sign ($^{\#}P < 0.05$; $^{\#\#}P < 0.01$). (D) Number of Iba1^{+} cells in the CA1/CA2 layers of the ipsilateral hippocampus. Note the significant reduction in such cells in infected PLX5622-treated mice. (E) Number of Iba1^{+} cells in the CA3c layer of the ipsilateral hippocampus. (F) Number of Iba1/Mac-3 double-labeled cells in the CA1/CA2 layers of the ipsilateral hippocampus. (G) Number of Iba1/Mac-3 double-labeled cells in the CA3c layer of the ipsilateral hippocampus. (H) Activation percentage in the CA1/CA2 layers of the ipsilateral hippocampus. (I) Activation percentage in the CA3c layer of the ipsilateral hippocampus. Note the higher percentage of Iba1/Mac-3 double labeled cells in infected PLX5622-treated mice. (For interpretation of the references to colour in this figure legend, the reader is referred to the web version of this article.)

3.8. CSF1R inhibition increases morbidity and mortality in the TMEV model

In infected B6 vehicle controls, animals did not show any signs of severe impairment due to infection and the following encephalitis as demonstrated by the Total Clinical Score (TCS) and weight development during the first days after infection (Fig. 10A). However, this strikingly changed in the PLX5622 treated group starting from day five post-infection (Fig. 10A). Animals showed severe paralysis of the hind limbs (Fig. 10B), bent-back posture, and a strong decrease in activity and food uptake. This health impairment was also displayed by severe loss of weight (Fig. 10C). Hence, some animals, which strongly showed these symptoms, had to be sacrificed before day seven to avoid suffering. Furthermore, one animal of the PLX5622-treated group died following infection. Survival analysis resulted in a highly significant difference between infected B6 vehicle controls and PLX5622-treated mice (Fig. 10D).

3.9. CSF1R inhibition facilitates seizure induction in the TMEV model

When determining the daily incidence of seizures across the 7 days after infection, maximum seizure occurrence was reached significantly more rapidly in PLX5622-treated mice than in vehicle controls, indicating that microglia depletion facilitated seizure induction (Fig. 11A). However, overall seizure incidence was not affected by microglia depletion: about 68% of the infected B6 vehicle controls exhibited seizures in the first week after infection compared to 78% of the PLX5622-treated group, which was not significantly different (Fig. 11B). No seizures were observed in the mock-infected groups. Most infected mice exhibited several seizures, but no significant intergroup difference in seizure frequency was observed (Fig. 11C). Similarly, the maximum seizure severity was not different in the two infected groups (Fig. 11D).

3.10. CSF1R inhibition alters cytokine and interferon mRNA expression in brain and spinal cord

In a series of previous studies in TMEV-infected B6 mice, release of the proinflammatory cytokines TNF-α and IL-6 by invading monocytes was described as particularly important for the seizure phenotype of these mice (DePaula-Silva et al., 2017). When these two cytokines were determined by RT-qPCR in the present study, significant increases in IL-6 and TNF-α mRNAs were observed in the brain (Fig. 12A, Supplemental Fig. S3A) and spinal cord (Fig. 12D, Supplemental Fig. S3E) of infected control mice. In infected PLX5622-treated mice, the brain increase in IL-6 was 20-fold more marked than the increase determined in infected controls (Fig. 12A), indicating increased release of this cytokine by invading monocytes. In addition to IL-6, a 6.6-fold more marked increase in expression of IL-10 was determined in the brain of infected PLX5622-treated mice compared to infected controls (Fig. 12B). Furthermore, a 2.3-fold more marked increase in expression of IFNγ was determined in the brain of infected PLX5622-treated mice compared to infected controls (Fig. 12C). In the spinal cord, the increase of IFNγ in infected PLX5622-treated mice was 49-fold higher than the increase determined in infected controls (Fig. 12F).

No marked differences between groups with or without PLX5622 were observed for IL-1β, IL-34, and TGF-β1 (Supplemental Fig. S3). IL-17 was below detection level in both mock and TMEV infected mice, including PLX5622 treated animals. Supplemental Fig. S4 summarizes the selective increases in cytokine and interferon mRNA levels in infected PLX5622-treated mice vs. infected controls, demonstrating the preferential increase of IL-6, IL-10 and IFNγ in the brain and IFNγ in the spinal cord of PLX5622-treated mice. Since IFNγ is preferentially released by cytotoxic CD8^{+} T cells whereas IL-10 is released by Tregs in the infected brain (Oleszak et al., 2004; DePaula-Silva et al., 2017), we calculated the ratio between the increase in IFNγ and IL-10 in the brain of infected controls vs. infected PLX5622-treated mice. This ratio was 5.57 in infected controls, indicating higher functionality of T effector cells vs. Tregs as regularly observed in TMEV-infected B6 mice (DePaula-Silva et al., 2017), whereas the ratio was 0.84 after in infected PLX5622-treated mice, indicating suppression of T effector cells by activated Tregs.

4. Discussion

Intracerebral infection of B6 mice with Theiler's virus is the first, and currently only, rodent model of viral encephalitis-induced seizures and epilepsy (Vezzani et al., 2016; DePaula-Silva et al., 2017). This model is ideally suited to investigate the mechanisms underlying the generation of seizures and hippocampal pathology developing during and after viral encephalitis. In contrast to B6 mice, which rapidly clear the virus, the virus persists in the CNS of SJL/J mice, which do not develop seizures and hippocampal damage, but a slowly progressing inflammatory demyelination in the spinal cord, making the TMEV infection in SJL/J mice a widely used model of multiple sclerosis (Oleszak et al., 2004; Procaccini et al., 2015; DePaula-Silva et al., 2017). While TMEV persistence in SJL/J mice is important to induce chronic demyelination, the trigger mechanism for demyelination is inflammation and the induction of autoimmunity (DePaula-Silva et al., 2017). The persistence of TMEV in the CNS of SJL/J mice is thought to be related, at least in part, to the high induction of Tregs during the acute stage of the infection, because Tregs can secrete immunosuppressive cytokines (such as IL-10), thereby blocking activation and effector function of cytotoxic CD8^{+} T cells that are important for viral clearance (Richards et al., 2011). In contrast to SJL/J mice, the lower number of Tregs induced in B6 mice after TMEV infection has been suggested to allow for rapid viral clearance by CD8^{+} T effector cells (Richards et al., 2011).

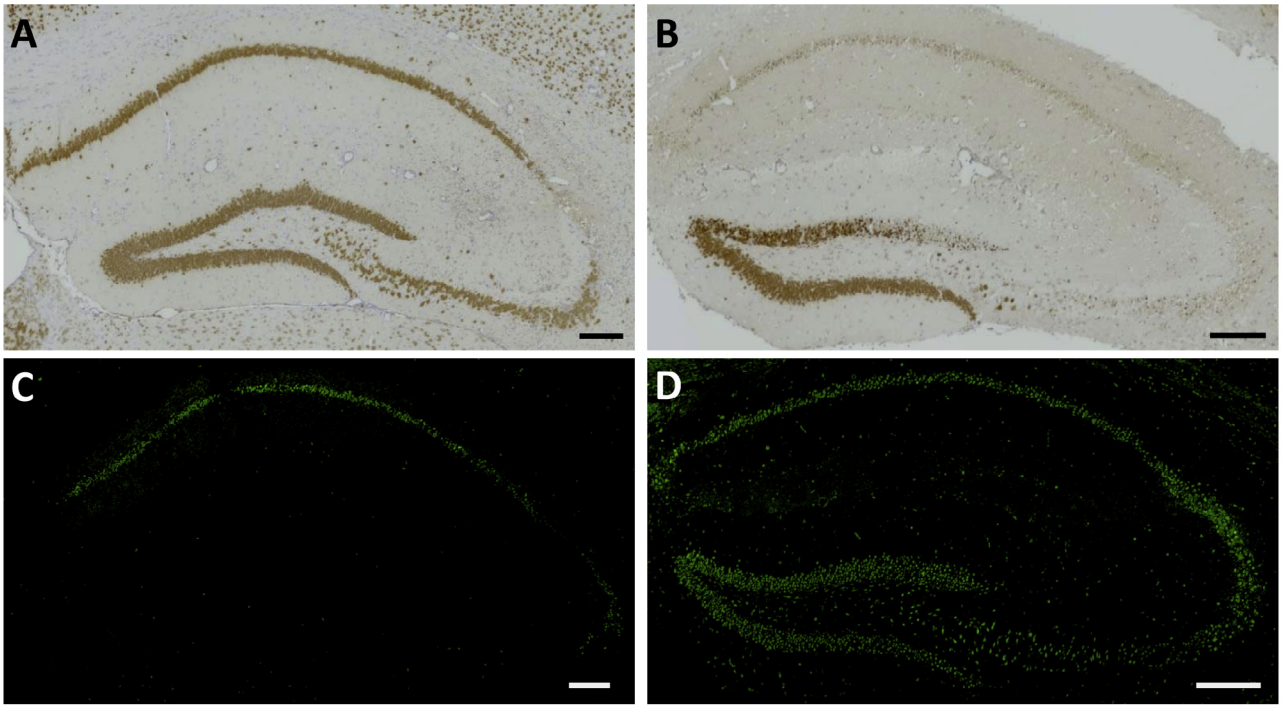

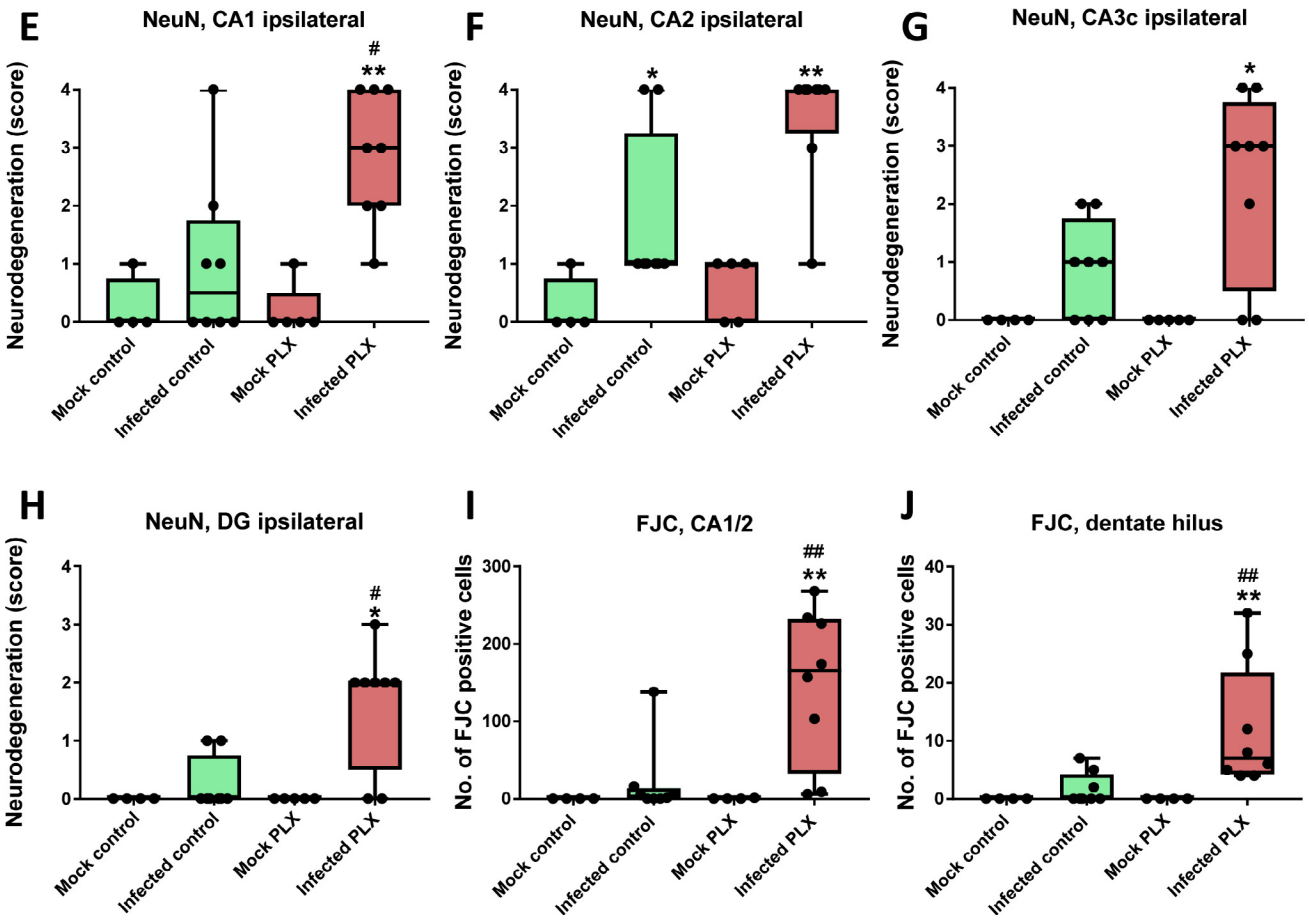

(caption on next page)

Fig. 8. Neurodegeneration in the hippocampus of infected mice. (A) Illustrates neuron staining by NeuN in an infected control mouse. Neurodegeneration is restricted to the CA2 sector of the hippocampus. (B) Illustrates neuron staining by NeuN in an infected PLX5622-treated mouse. Neurodegeneration affects all hippocampal neuronal layers, including CA1, CA2, CA3, dentate hilus, and part of the granule cell layer of the dentate gyrus. (C) Illustrates labeling of dying neurons by Fluoro-Jade C (FJC; green) in an infected control mouse. Only neurons in part of the CA1 and CA2 layers are labeled. (D) Illustrates labeling of dying neurons by FJC in an infected PLX5622-treated mouse. Neurons in all parts of the hippocampus are labeled, including CA1, CA2, CA3, and hilus and granule cell layer of the dentate gyrus. Scale bars in A-D = 200 μm. (E–J) Quantitative data for neuronal labeling by NeuN (E–H) or FJC (I, J). Data are shown as boxplots with whiskers from minimum to maximal values; the horizontal line in the boxes represents the median value. In addition, individual data are shown. Sample size: 4 mock-infected controls; 4–5 mock-infected mice with PLX5622; 8 infected controls; 8 infected mice with PLX5622. Significant differences to mock-infected mice are indicated by asterisks ($^{*}P < 0.05$; $^{**}P < 0.01$) while significant differences between infected mice treated with PLX5622 and infected controls are indicated by the hash sign ($^{\#}P < 0.05$; $^{\#\#}P < 0.01$). (E) Shows the increased neurodegeneration in infected PLX5622-treated mice in the ipsilateral CA1 layer of the hippocampus. (F) Shows that neurodegeneration in the CA2 layer of the ipsilateral hippocampus does not differ between infected controls and infected PLX5622-treated mice. (G) Shows the increased neurodegeneration in infected PLX5622-treated mice in the ipsilateral CA3c layer of the hippocampus. (H) Shows the increased neurodegeneration in infected PLX5622-treated mice in the ipsilateral dentate gyrus (DG) layer of the hippocampus. (I) shows the increased number of dying neurons in infected PLX5622-treated mice in the ipsilateral CA1/CA2 layers of the hippocampus. (J) Shows the increased number of dying neurons in infected PLX5622-treated mice in the ipsilateral dentate hilus of the hippocampus. (For interpretation of the references to colour in this figure legend, the reader is referred to the web version of this article.)

Indeed, Tregs, characterized by expression of the transcription factor forkhead box P3 (Foxp3), are known to modulate the immune response to viral infection, and numerous infection models have demonstrated that Treg depletion increases viral clearance and IFNγ production by $CD8^+$ T cells (Groux et al., 1997; Dittmer et al., 2004; He et al., 2004; Eggena et al., 2005). However, in TMEV-infected B6 mice, ablation of $Foxp3^+$ Tregs during the acute disease phase of TMEV infection did not accelerate virus clearance (Prajeeth et al., 2014). In contrast, ablation of cytotoxic $CD8^+$ T cells rendered B6 mice susceptible to develop chronic demyelinating neuroinfection comparable to the encephalomyelitis observed in SJL/J mice, which might partly be mediated by boosting the suppressive capacity of Tregs on viral elimination (Ciurkiewicz et al., 2017).

In addition to $CD8^+$ T cells, it has been suggested that $CD4^+$ T cells may confer protection against TMEV persistence and demyelination in resistant mouse strains such as B6 (Murray et al., 1998; Kang et al., 2005; Mohindru et al., 2006). Indeed, genetic deletion of either $CD4^+$ or $CD8^+$ cells from B6 mice resulted in viral persistence and demyelination during the chronic stage of disease (Murray et al., 1998). Interestingly, neither $CD4^+$ nor $CD8^+$ cells are required for development of acute seizures following infection with TMEV in B6 mice (DePaula-Silva et al., 2018).

The present study shows that depletion of microglia is an effective means to retard viral clearance and exacerbate the TMEV-induced disease in B6 mice, thus defining the role of microglia in this model of viral encephalitis. Previously, understanding the roles that microglia play in a neurotropic viral infection and how these roles affect the immune response to viruses has been complicated by differentiating microglia from extensively infiltrating monocytes with potentially overlapping functions during neuroinflammation (Terry et al., 2012; Prinz and Priller, 2014; Prinz et al., 2017). Furthermore, while microglia, the resident macrophages of the CNS, are often touted as the first responders to a CNS viral infection and are known to respond rapidly to injury (Rock et al., 2004; Carrithers, 2014), there is little direct evidence to show that microglia are needed for an optimal host response to pathogens. Selective and complete depletion of microglia by chronic treatment with the CSF1R inhibitor PLX5622 is an ideal means to study the functions that microglia use in responding to viruses. PLX5622 is a potent inhibitor of CSF1R tyrosine kinase activity (Ki = 5.9 nM) with at least 50-fold selectivity over 4 related kinases, and over 100-fold selectivity against a panel of 230 kinases (Dagher et al., 2015). As shown here, by the PLX5622 treatment protocol used, CSF1R mRNA expression in the CNS was almost completely lost, which is a consequence of the depletion of microglia that express this mRNA.

Recent studies in the TMEV model in B6 mice have suggested that both seizures and hippocampal damage in this mouse strain are primarily due to infiltration of blood-derived monocytes and cytokines released by these cells (Howe et al., 2012a,b; Cusick et al., 2013), resulting in apoptotic death of neurons in the CA1/CA2 area of the hippocampus (Buenz et al., 2009; Howe et al., 2012b). Indeed, suppression of monocyte infiltration by deleting the chemokine receptor CCR2 prevented hippocampal damage following TMEV infection, but did not prevent encephalitis-associated seizures (Käufer et al., 2018), thus challenging previous assumptions with less selective approaches (Cusick et al., 2013). The present study shows that depletion of microglia by PLX5622 exacerbates hippocampal damage and increases progression of seizures following viral encephalitis, indicating that microglia may exhibit a protective role in this model, at least in the early phase following infection. Furthermore, neuronal damage, associated with severe motor impairment, occurred in the spinal cord, which is typically not affected in B6 mice. The severe clinical impairment and enhanced mortality in infected mice treated with PLX5622 did not allow evaluating whether spinal cord demyelination occurs at later stages of the infection as observed in TMEV-infected SJL/J mice.

The first study that reported the effect of microglia depletion in B6 mice on viral encephalitis used intracranial infection with a neuroattenuated variant of the JHMV strain of MHV (Wheeler et al., 2018), which induces mild acute encephalitis and acute and chronic demyelinating disease (Bergmann et al., 2006). Treatment with PLX5622 increased CNS replication of MHV and subsequent mortality in B6 mice, which was explained by ineffective innate and virus-specific T cell responses resulting from microglia depletion (Wheeler et al., 2018). Indeed, microglia depletion led to a markedly reduced brain infiltration of $CD4^+$ T cells and $Foxp3^+$ Tregs as well as IFNγ expression at 7 days after infection (Wheeler et al., 2018). The present data show that these consequences of microglia depletion are virus specific, because we did not observe a decrease but a significant increase in infiltration of $Foxp3^+$ Tregs in hippocampus and spinal cord and only a relatively small reduction in brain invasion of $CD4^+$ T cells in TMEV-infected, PLX5622-treated mice compared to infected controls, although the invasion of $CD4^+CD44^+$ T cells was markedly reduced by microglia depletion. Furthermore, in apparent contrast to the study of Wheeler et al. (2018), IFNγ expression was significantly increased in brain and spinal cord of PLX5622-treated mice in response to TMEV infection.

In a recent study using PLX5622 for determining the role of microglia in flaviviral pathogenesis in female Swiss-Webster mice (Seitz et al., 2018), depletion of microglia resulted in increased mortality and viral titer in the brain following infection with either West Nile virus (WNV) or Japanese encephalitis virus (JEV). Interestingly, the expression of several pro-inflammatory genes was increased in virus-infected, microglial-depleted mice compared to virus-infected, untreated controls. T cell responses were not examined in the study of Seitz et al. (2018).

In both previous studies on depleting microglia in viral CNS infection models, Iba1 was used as a marker for microglia (Seitz et al., 2018; Wheeler et al., 2018). However, Iba1 is not selective for microglia but also labels monocytes that invade the brain during viral encephalitis (Greter et al., 2015), which is also shown here. For the present study,

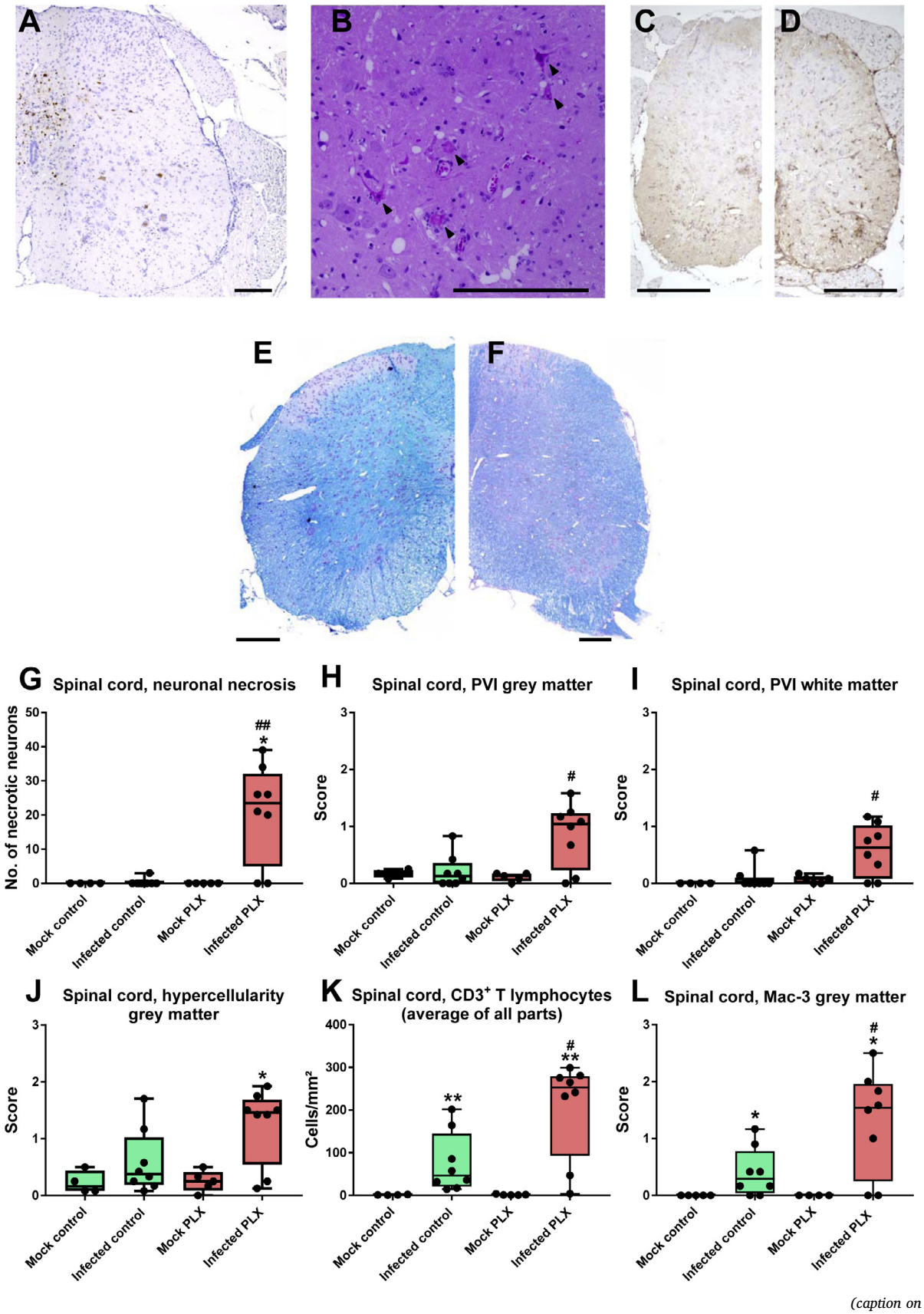

(caption on next page)

Fig. 9. Neuroinflammation and neurodegeneration in the spinal cord. (A) A representative photomicrograph of virus antigen staining in the spinal cord of an infected PLX5622-treated mouse. No such staining was observed in infected controls (see Fig. 5F for quantitative data). (B) Neuronal necrosis in the spinal cord (arrows) as indicated in H&E-stained sections of an infected PLX5622-treated mouse. (C) Mac-3 labeled cells in the spinal cord of an infected control. (D) Mac-3 labeled cells in the spinal cord of an infected PLX5622-treated mouse; note the increase in Mac-3 labeled cells vs. (C). (E) Luxol fast blue (LFB) staining of myelin in the spinal cord of an infected control. (F) LFB staining in the spinal cord of an infected PLX5622-treated mouse. No indication of demyelination was observed in E or F. (G-L) Quantitative data for neuronal necrosis (G), perivascular infiltrates (PVI; H, I), hypercellularity (J), $CD3^+$ T lymphocyte infiltration (K), and Mac-3 labeled cells (L). Data are shown as boxplots with whiskers from minimum to maximal values; the horizontal line in the boxes represents the median value. In addition, individual data are shown. Sample size: 4 mock-infected controls; 5 mock-infected mice with PLX5622; 8 infected controls; 8 infected mice with PLX5622. Significant differences to mock-infected mice are indicated by asterisks ($^{*}P < 0.05$; $^{**}P < 0.01$) while significant differences between infected mice treated with PLX5622 and infected controls are indicated by the hash sign ($^{\#}P < 0.05$; $^{\#\#}P < 0.01$). All parameters shown in G-L demonstrated the increased neuroinflammation and neurodegeneration induced by treatment with PLX5622 in the spinal cord of C57BL/6 (B6) mice. All scale bars = 200 μm. (For interpretation of the references to colour in this figure legend, the reader is referred to the web version of this article.)

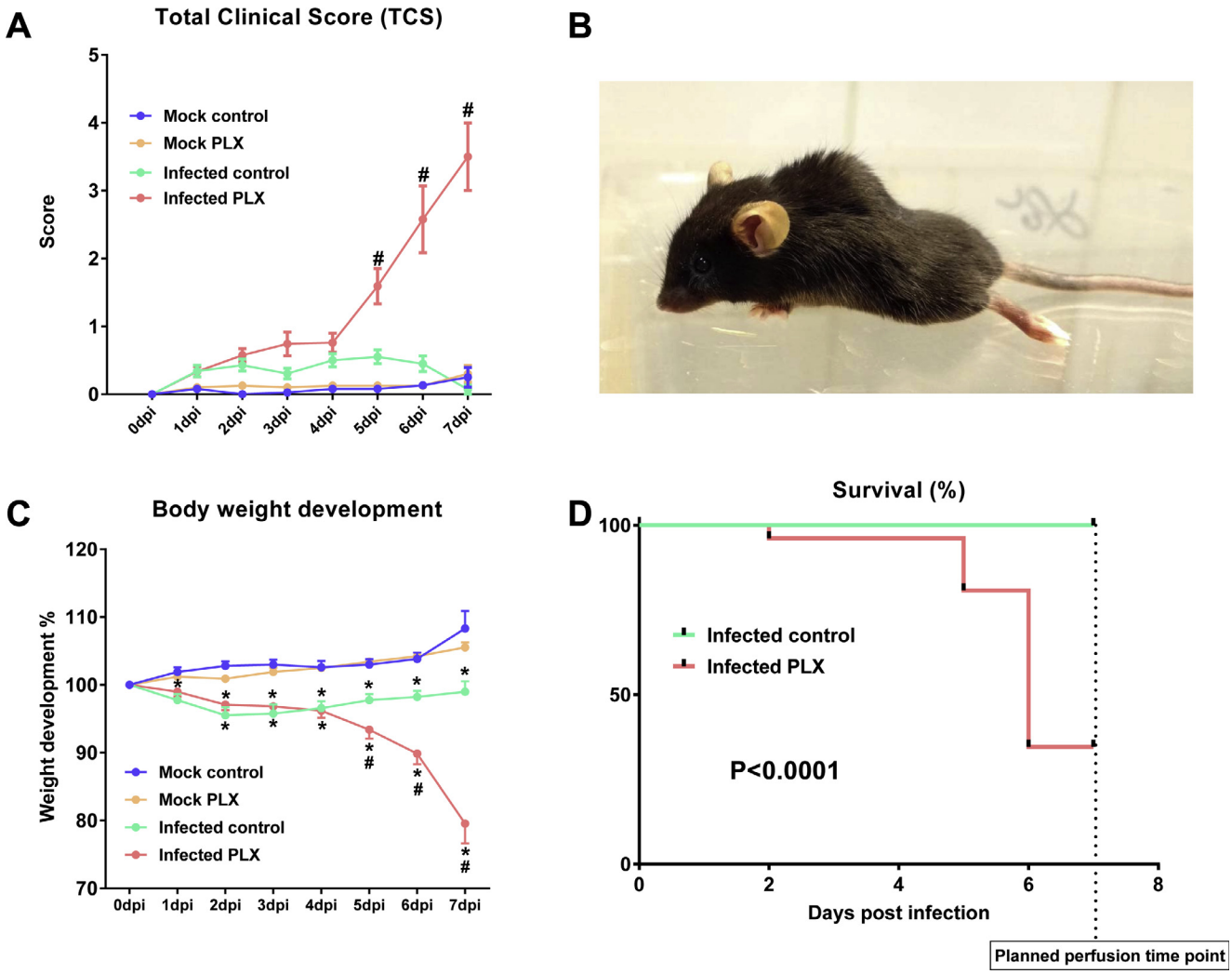

Fig. 10. Clinical data from infected mice. Experiments were performed several times (see Fig. 1) and data summarized; sample size: 19 mock-infected controls; 20 mock-infected mice with PLX5622; 28 infected controls; 27 infected mice with PLX5622. (A) Illustrates the "total clinical score", describing the overall clinical impairment, ranging from 0 (healthy) to 10 (maximal clinical impairment) (see Methods). Infected controls did not differ from mock-infected controls (except for seizures, which were assessed separately as shown in Fig. 11), while infected PLX5622-treated mice developed severe clinical symptoms, including paralysis of the hind limbs, bent-back posture, and a strong decrease in general activity and food uptake. Data are shown as means ± SEM and were analyzed by two-way ANOVA; significant differences between infected PLX5622-treated mice to all other groups are indicated by the hash sign ($^{\#}P < 0.0001$). (B) A representative picture of a PLX5622-treated infected mouse with paralysis of hind limbs, which was never observed in infected controls. (C) Body weight development. Data are shown as means ± SEM and were analyzed by two-way ANOVA; significance between infected and mock-infected mice is indicated by asterisk ($^{*}P < 0.01$), while significance between PLX5622-treated and vehicle-treated infected mice is indicated by the hash sign ($^{\#}P < 0.01$). Note the much more severe weight loss in infected PLX5622-treated mice. (D) Survical curves for infected controls and infected PLX5622-treated mice. Mice that had to be killed before day 7 (the planned end of the experiment) because of poor health status were included in survival analysis. Statistical evaluation of data by the log-rank (Mantel-Cox) test indicated a highly significant ($P < 0.0001$) difference between groups.

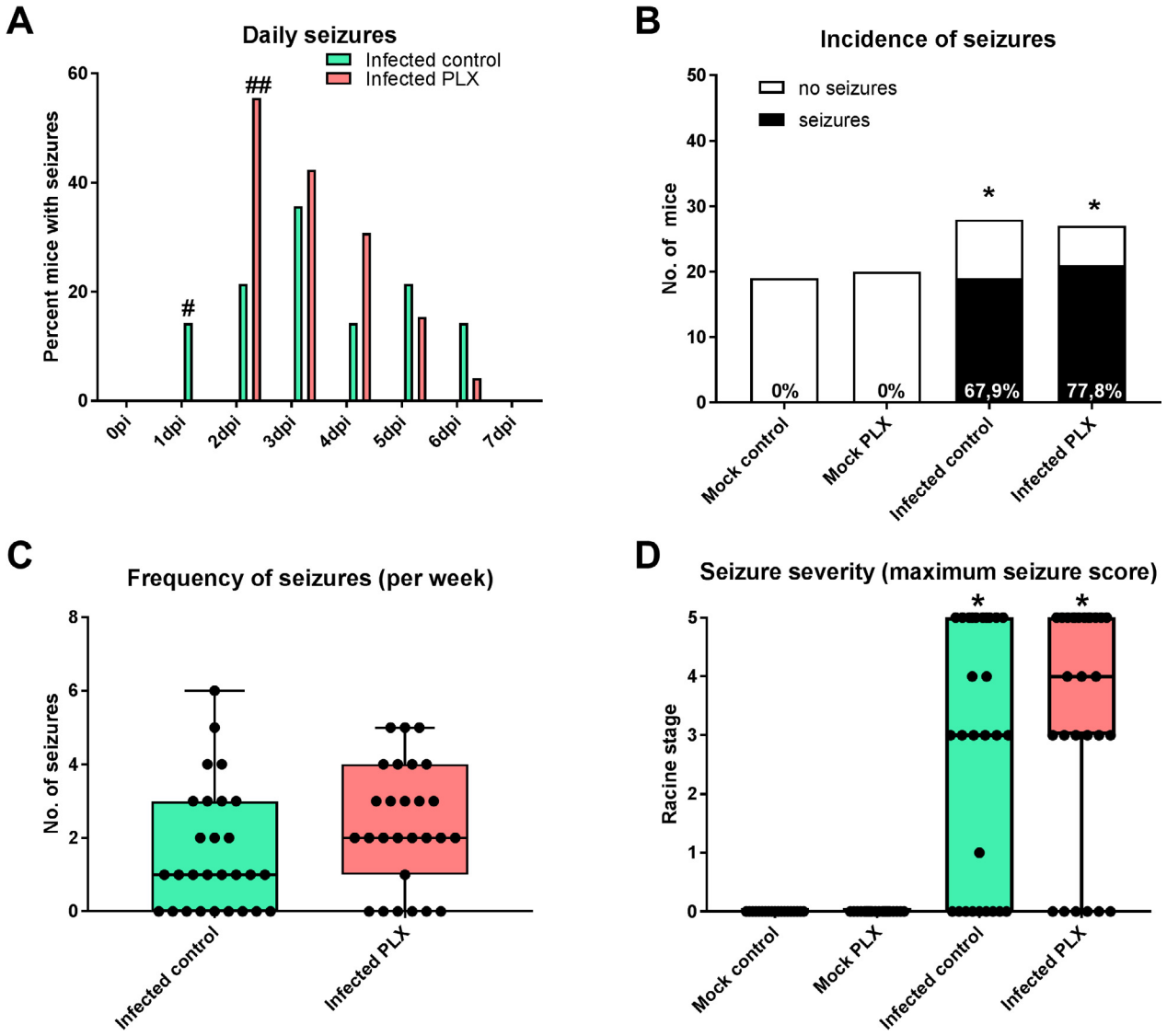

Fig. 11. Insult-associated seizures monitored in the first week after infection. Experiments were performed several times (see Fig. 1) and data summarized; sample size: 19 mock-infected controls; 20 mock-infected mice with PLX5622; 28 infected controls; 27 infected mice with PLX5622. (A) Occurrence of acute (early) seizures in the 6–7 days after infection. Data are shown as percent of mice with seizures per mice infected with Theiler's DA virus for each experimental day. Significant intergroup differences are indicated by the hash sign ($^{\#}P < 0.05$; $^{\#\#}P < 0.01$). (B) illustrates the incidence of seizures in the four groups, showing that none of the noninfected controls exhibited seizures whereas 10/15 infected controls and 11/14 infected PLX-treated mice exhibited seizures, which both was significantly different from noninfected controls (indicated by asterisks; $^{*}P < 0.0001$). (C) Frequency of seizures recorded in infected mice. Data are shown as boxplots with whiskers from minimum to maximal values; the horizontal line in the boxes represents the median value; in addition, individual data are shown. No intergroup difference was found. (D) Seizure severity as indicated by the maximum seizure score for each mouse with seizures. Data are shown as boxplots with whiskers from minimum to maximal values; the horizontal line in the boxes represents the median value; in addition, individual data are shown. Significant differences to noninfected controls are indicated by asterisks ($^{*}P < 0.001$). No intergroup difference was found in the experiment illustrated in D.

we chose the much more selective microglia marker TMEM119 (Bennett et al., 2016), demonstrating that PLX5622 results in complete microglia depletion at the chosen dosing protocol. This was confirmed by flow cytometry.

CSF1R, the receptor affected by PLX5622, is also expressed on other myeloid cells, including brain perivascular macrophages and infiltrating hematopoietic monocytes (Hamilton and Achuthan, 2013). As a consequence, we observed a significant decrease in circulating $CSF1R^{+}$ monocytes in the blood of mock infected mice after treatment with PLX5622. After infection, blood $CSF1R^{+}$ monocytes increased in both controls and PLX5622-treated groups, although to a slightly lower degree in the PLX5622-treated mice. This was not associated with any obvious reduction in brain infiltration of blood-derived monocytes as both demonstrated by flow cytometry and immunolabeling by Mac-3 and Iba1. Instead, both Mac-3 and Iba1 indicated an increase of myeloid cells in the hippocampus and spinal cord of infected mice after depletion of microglia, indicating that infiltrating hematopoietic monocytes/macrophages try to compensate for the lack of microglia. In line with this idea, mRNA expression of IL-6, which is released by both invading monocytes and activated microglia (Oleszak et al., 2004), was increased 20-fold in microglia-depleted brains of infected mice.

Interleukin-6 (IL-6) plays an important role in the development and progression of inflammatory responses, in part by facilitating the generation of IL-17-producing Th17 cells (Kothur et al., 2016). Many viral infections, including TMEV, result in the vigorous production of IL-6 (Kothur et al., 2016; DePaula-Silva et al., 2017). B6 mice carrying an IL-6 transgene, resulting in the production of excessive IL-6, develop a TMEV-induced demyelinating disease accompanied by an increase in viral persistence and an elevated Th17 cell response in the CNS (Hou et al., 2014). IL-17 producing Th17 cells have been shown to promote

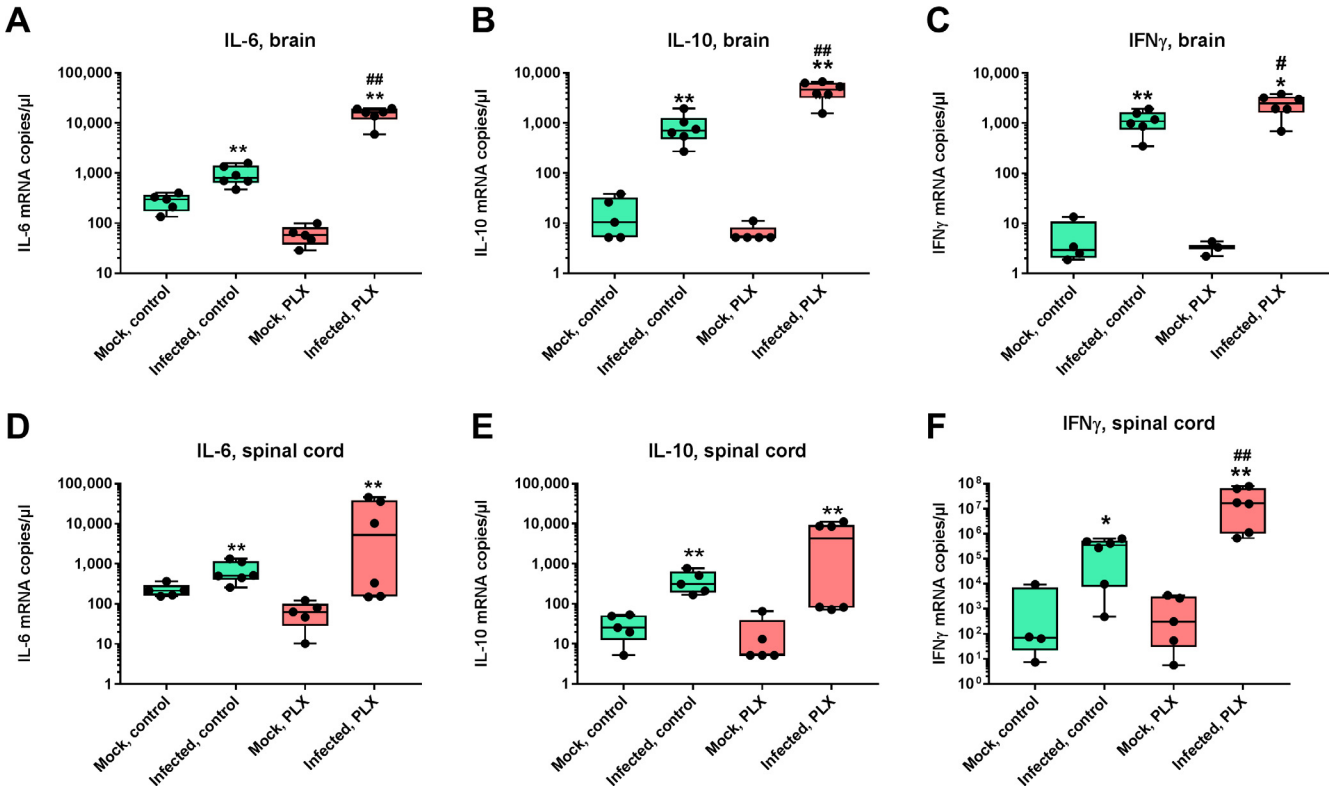

Fig. 12. TNFα, IL-6, and IFNγ mRNA expression in brain and spinal cord of infected mice. Data are shown as boxplots with whiskers from minimum to maximal values; the horizontal line in the boxes represents the median value. Note that y-axis has a logarithmic scale. In addition, individual data are shown. Sample size is 5 for noninfected mice and 6 for infected mice. Significant differences to mock-infected mice are indicated by asterisks ($^{*}P < 0.05$; $^{**}P < 0.01$) while significant differences between infected mice treated with PLX5622 and infected controls are indicated by the hash sign ($^{\#}P < 0.05$; $^{\#\#}P < 0.01$). (A) TNFα mRNA expression in brain. (B) IL6 mRNA expression in brain. (C) IFNγ mRNA expression in brain. (D) TNFα mRNA expression in spinal cord. (E) IL6 mRNA expression in spinal cord. (F) IFNγ mRNA expression in spinal cord.

persistent viral infection by inhibiting cytotoxic T cell function and apoptotic cell death (Hou et al., 2009). As shown by Hou et al. (2014), excessive IL-6 promotes the generation of Th17 cells, and the resulting IL-6 and IL-17 synergistically promote viral persistence by protecting virus-infected cells from apoptosis and $CD8^+$ T cell-mediated target destruction. These data suggest that the 20-fold increase in IL-6 following microglia depletion by PLX5622 may be involved in the altered responses to TMEV infection observed in the present experiments. However, we did not observe an increase in IL-17 in microglia-depleted mice following TMEV infection, demonstrating low numbers of Th17 cells in this early phase of the disease (6–7 days p.i.).

Instead, we observed a marked increase in brain mRNA expression of the immunosuppressive cytokine IL-10 in the brain of infected PLX5622-treated mice compared to infected B6 controls. Among other cell types, IL-10 is secreted by Tregs, which were significantly increased in the brain of infected PLX5622-treated mice. Thus, similar to TMEV infection in SJL/J mice, microglia depletion in B6 mice seems to lead to an unfavorable ratio between Tregs and T effector cells, resulting in suppression of T cell activation and effector function. This interpretation of the data was substantiated when calculating the ratio between IFNγ and IL-10 in the brain of infected controls vs. infected mice treated with PLX5622, demonstrating a reversal in this ratio from 5.57 to 0.84. This indicates that IL-10 suppressed functionality of IFNγ-releasing T effector cells following microglia depletion.

In the spinal cord, however, a massive, 50-fold increase of IFNγ was observed. This increase in IFNγ may be critically involved in disease exacerbation. In neuroinflammatory CNS disorders, IFNγ is elevated mainly in viral encephalitis, suggesting activation of lymphocytes in the CNS which participate in viral clearance (Kothur et al., 2016). IFNγ, which is produced by activated natural killer (NK) and T cells, is important for virus clearance and induces many immunomodulatory effects, including activation of macrophages, promotion of leukocyte adhesion to allow trafficking of cells to the CNS, direct antiviral and antiproliferative effects, and induction of the release of other cytokines, including TNF-α and IL-1 (Bowen and Olson, 2013). IFNγ has been implicated in the clearance of virus from CNS following infection with a wide variety of viruses, including TMEV (Rodriguez et al., 2003). However, at high concentrations as observed following microglia depletion here, IFNγ is neurotoxic through a neuron specific, calcium-permeable complex of IFNγ-receptor and the AMPA subtype of glutamate receptors (Mizuno et al., 2008). Thus, IFNγ in concert with other cytokines such as IL-6β may contribute to the increased degeneration of hippocampal and spinal cord motor neurons and clinical signs observed after microglia depletion in TMEV-infected mice.

This, however, does not necessarily explain the facilitation of seizures observed in infected PLX5622-treated mice. Here, a direct effect of microglia could be important. By debris clearance and continuously contacting dendritic spines to regulate structural synaptic changes, microglia plays a fundamental role in facilitating the reorganization of neuronal circuits and triggering repair in CNS injury (Neumann et al., 2009; Kim et al., 2013). Proper synaptic pruning (or engulfment) by microglia has been shown to modulate seizure threshold (Kim et al., 2013), which could explain the facilitated seizure induction observed after microglia depletion in Theiler's virus-infected mice.

Overall, based on the present data, the following scenario can be postulated. Depletion of microglia reduces the local immune response to infection, resulting in increased virus proliferation. Enhanced induction of Tregs in hippocampus and spinal cord and resulting IL-10 release seem to add to the reduced immune response to viral infection observed after microglia depletion. On the other hand, markedly

increased IL-6, and, in the spinal cord, IFNγ levels contribute to neurodegeneration and elevated seizure susceptibility. Also, the increased astrogliosis observed in infected, microglia-depleted mice may contribute to neuroinflammation and related processes, although a neurotoxic subtype (A1) of astrocytes, which is induced by neuroinflammatory microglia (Liddelow et al., 2017), should be reduced or absent in microglia-depleted mice. Our results demonstrate a critical role for microglia in the context of viral encephalitis, affecting virus replication and innate and adaptive immune responses as well as disease progression and severity. However, as indicated by the significant differences in response to microglia depletion between the study of Wheeler et al. (2018) with a coronavirus (MHV) and the present study with a picornavirus (TMEV), both performed in B6 mice, the role of microglia in viral encephalitis markedly depends on the specific virus inducing the disease. Furthermore, the severity of viral encephalitis certainly has an impact on specific microglia response. The present findings enhance our understanding of microglia-T cell crosstalk that seems to play a vital role in neuroinflammation, whether through soluble mediators or *via* contact-dependent interactions (Schetters et al., 2017).

Author contributions

IW and WL conceived the study; IW, CK, IG, CC and LG acquired and validated the data and executed the experiments; IW, CK, IG, CC, LG, and WL analyzed the data; WL wrote the manuscript and all authors revised the manuscript.

Conflict of interest

The authors declare no competing financial interests.

Acknowledgements

We thank Prof. Robert S. Fujinami for providing the DA strain of TMEV, Plexxikon for providing PLX5622, Prof. Andreas Beineke for helpful discussion on a previous version of the manuscript, and Edith Kaczmarek, Caroline Schütz, Danuta Waschke, Petra Grünig, Muneeb Anjum, Alina Schidlitzki for skillful technical assistance. The study was supported by the Niedersachsen-Research Network on Neuroinfectiology (N-RENNT) of the Ministry of Science and Culture of Lower Saxony in Germany and the Helmholtz “Zukunftsthema Immunology & Inflammation”. Chintan Chhatbar was supported by a bilateral project of the German Centre for Neurodegenerative Diseases and the Helmholtz Centre for Infection Research (to U.K.) and by the Niedersachsen-Research Network on Neuroinfectiology (N-RENNT) of the Ministry of Science and Culture of Lower Saxony, Germany (to U.K.).

Appendix A. Supplementary data

Supplementary data to this article can be found online at https://doi.org/10.1016/j.bbi.2018.09.006.

References

Acharya, M.M., Green, K.N., Allen, B.D., Najafi, A.R., Syage, A., Minasyan, H., Le, M.T., Kawashita, T., Giedzinski, E., Parihar, V.K., West, B.L., Baulch, J.E., Limoli, C.L., 2016. Elimination of microglia improves cognitive function following cranial irradiation. Sci. Rep. 6, 31545.

Baaten, B.J., Li, C.R., Bradley, L.M., 2010. Multifaceted regulation of T cells by CD44. Commun. Integr. Biol. 3, 508–512.

Beckers, L., Stroobants, S., Verheijden, S., West, B., D'Hooge, R., Baes, M., 2017. Specific suppression of microgliosis cannot circumvent the severe neuropathology in peroxisomal beta-oxidation-deficient mice. Mol. Cell Neurosci. 80, 123–133.

Bennett, M.L., Bennett, F.C., Liddelow, S.A., Ajami, B., Zamanian, J.L., Fernhoff, N.B., Mulinyawe, S.B., Bohlen, C.J., Adil, A., Tucker, A., Weissman, I.L., Chang, E.F., Li, G., Grant, G.A., Hayden Gephart, M.G., Barres, B.A., 2016. New tools for studying microglia in the mouse and human CNS. Proc. Natl. Acad. Sci. U.S.A. 113, E1738–E1746.

Bergmann, C.C., Lane, T.E., Stohlman, S.A., 2006. Coronavirus infection of the central nervous system: host-virus stand-off. Nat. Rev. Microbiol. 4, 121–132.

Bowen, J.L., Olson, J.K., 2013. IFNgamma influences type I interferon response and susceptibility to Theiler's virus-induced demyelinating disease. Viral Immunol. 26, 223–238.

Bröer, S., Kaufer, C., Haist, V., Li, L., Gerhauser, I., Anjum, M., Bankstahl, M., Baumgärtner, W., Löscher, W., 2016. Brain inflammation, neurodegeneration and seizure development following picornavirus infection markedly differ among virus and mouse strains and substrains. Exp. Neurol. 279, 57–74.

Bröer, S., Hage, E., Käufer, C., Gerhauser, I., Anjum, M., Li, L., Baumgärtner, W., Schulz, T.F., Löscher, W., 2017. Viral mouse models of multiple sclerosis and epilepsy: Marked differences in neuropathogenesis following infection with two naturally occurring variants of Theiler's virus BeAn strain. Neurobiol. Dis. 99, 121–132.

Buenz, E.J., Sauer, B.M., Lafrance-Corey, R.G., Deb, C., Denic, A., German, C.L., Howe, C.L., 2009. Apoptosis of hippocampal pyramidal neurons is virus independent in a mouse model of acute neurovirulent picornavirus infection. Am. J. Pathol. 175, 668–684.

Carrithers, M.D., 2014. Innate immune viral recognition: relevance to CNS infections. Handb. Clin. Neurol. 123, 215–223.

Ciurkiewicz, M., Herder, V., Khan, M.A., Uhde, A.K., Teich, R., Floess, S., Baumgartner, W., Huehn, J., Beineke, A., 2017. Cytotoxic CD8(+) T cell ablation enhances the capacity of regulatory T cells to delay viral elimination in Theiler's murine encephalomyelitis. Brain Pathol.

Cusick, M.F., Libbey, J.E., Patel, D.C., Doty, D.J., Fujinami, R.S., 2013. Infiltrating macrophages are key to the development of seizures following virus infection. J. Virol. 87, 1849–1860.

Dagher, N.N., Najafi, A.R., Kayala, K.M., Elmore, M.R., White, T.E., Medeiros, R., West, B.L., Green, K.N., 2015. Colony-stimulating factor 1 receptor inhibition prevents microglial plaque association and improves cognition in 3xTg-AD mice. J. Neuroinflammation 12, 139.

DePaula-Silva, A.B., Hanak, T.J., Libbey, J.E., Fujinami, R.S., 2017. Theiler's murine encephalomyelitis virus infection of SJL/J and C57BL/6J mice: Models for multiple sclerosis and epilepsy. J. Neuroimmunol. 308, 30–42.

DePaula-Silva, A.B., Sonderegger, F.L., Libbey, J.E., Doty, D.J., Fujinami, R.S., 2018. The immune response to picornavirus infection and the effect of immune manipulation on acute seizures. J. Neurovirol in press.

Dittmer, U., He, H., Messer, R.J., Schimmer, S., Olbrich, A.R., Ohlen, C., Greenberg, P.D., Stromnes, I.M., Iwashiro, M., Sakaguchi, S., Evans, L.H., Peterson, K.E., Yang, G., Hasenkrug, K.J., 2004. Functional impairment of CD8(+) T cells by regulatory T cells during persistent retroviral infection. Immunity 20, 293–303.

Eggena, M.P., Barugahare, B., Jones, N., Okello, M., Mutalya, S., Kityo, C., Mugyenyi, P., Cao, H., 2005. Depletion of regulatory T cells in HIV infection is associated with immune activation. J. Immunol. 174, 4407–4414.

Elmore, M.R., Najafi, A.R., Koike, M.A., Dagher, N.N., Spangenberg, E.E., Rice, R.A., Kitazawa, M., Matusow, B., Nguyen, H., West, B.L., Green, K.N., 2014. Colony-stimulating factor 1 receptor signaling is necessary for microglia viability, unmasking a microglia progenitor cell in the adult brain. Neuron 82, 380–397.

Elmore, M.R., Lee, R.J., West, B.L., Green, K.N., 2015. Characterizing newly repopulated microglia in the adult mouse: impacts on animal behavior, cell morphology, and neuroinflammation. PLoS One 10, e0122912.

Erblich, B., Zhu, L., Etgen, A.M., Dobrenis, K., Pollard, J.W., 2011. Absence of colony stimulation factor-1 receptor results in loss of microglia, disrupted brain development and olfactory deficits. PLoS One 6, e26317.

Feng, X., Jopson, T.D., Paladini, M.S., Liu, S., West, B.L., Gupta, N., Rosi, S., 2016. Colony-stimulating factor 1 receptor blockade prevents fractionated whole-brain irradiation-induced memory deficits. J. Neuroinflammation 13, 215.

Gerhauser, I., Alldinger, S., Ulrich, R., Baumgärtner, W., 2005. Spatio-temporal expression of immediate early genes in the central nervous system of SJL/J mice. Int. J. Dev. Neurosci. 23, 637–649.

Gerhauser, I., Alldinger, S., Baumgartner, W., 2007. Ets-1 represents a pivotal transcription factor for viral clearance, inflammation, and demyelination in a mouse model of multiple sclerosis. J. Neuroimmunol. 188, 86–94.

Gerhauser, I., Hansmann, F., Puff, C., Kumnok, J., Schaudien, D., Wewetzer, K., Baumgartner, W., 2012. Theiler's murine encephalomyelitis virus induced phenotype switch of microglia in vitro. J. Neuroimmunol. 252, 49–55.

Greter, M., Lelios, I., Croxford, A.L., 2015. Microglia versus myeloid cell nomenclature during brain inflammation. Front Immunol. 6, 249.

Groux, H., O'Garra, A., Bigler, M., Rouleau, M., Antonenko, S., de Vries, J.E., Roncarolo, M.G., 1997. A CD4+ T-cell subset inhibits antigen-specific T-cell responses and prevents colitis. Nature 389, 737–742.

Gröticke, I., Hoffmann, K., Löscher, W., 2008. Behavioral alterations in a mouse model of temporal lobe epilepsy induced by intrahippocampal injection of kainate. Exp. Neurol. 213, 71–83.

Hamilton, J.A., Achuthan, A., 2013. Colony stimulating factors and myeloid cell biology in health and disease. Trends Immunol. 34, 81–89.

He, H., Messer, R.J., Sakaguchi, S., Yang, G., Robertson, S.J., Hasenkrug, K.J., 2004. Reduction of retrovirus-induced immunosuppression by in vivo modulation of T cells during acute infection. J. Virol. 78, 11641–11647.

Hilla, A.M., Diekmann, H., Fischer, D., 2017. Microglia are irrelevant for neuronal degeneration and axon regeneration after acute injury. J. Neurosci. 37, 6113–6124.

Hou, W., Kang, H.S., Kim, B.S., 2009. Th17 cells enhance viral persistence and inhibit T cell cytotoxicity in a model of chronic virus infection. J. Exp. Med 206, 313–328.

Hou, W., Jin, Y.H., Kang, H.S., Kim, B.S., 2014. Interleukin-6 (IL-6) and IL-17 synergistically promote viral persistence by inhibiting cellular apoptosis and cytotoxic T cell

function. J. Virol. 88, 8479–8489.
Howe, C.L., Lafrance-Corey, R.G., Sundsbak, R.S., Lafrance, S.J., 2012a. Inflammatory monocytes damage the hippocampus during acute picornavirus infection of the brain. J. Neuroinflammation 9, 50.
Howe, C.L., Lafrance-Corey, R.G., Sundsbak, R.S., Sauer, B.M., Lafrance, S.J., Buenz, E.J., Schmalstieg, W.F., 2012b. Hippocampal protection in mice with an attenuated inflammatory monocyte response to acute CNS picornavirus infection. Sci. Rep. 2, 545.
Kang, B., Kang, H.K., Kim, B.S., 2005. Identification of capsid epitopes of Theiler's virus recognized by CNS-infiltrating CD4+ T cells from virus-infected C57BL/6 mice. Virus Res. 108, 57–61.
Käufer, C., Chatbar, C., Bröer, S., Waltl, I., Luca, G., Gerhauser, I., Kalinke, U., Löscher, W., 2018. Chemokine receptors CCR2 and CX3CR1 regulate viral encephalitis-induced hippocampal damage but not seizures. Proc. Natl. Acad. Sci. U.S.A in press.
Kim, K.H., Son, S.M., Mook-Jung, I., 2013. Contributions of microglia to structural synaptic plasticity. J. Exp. Neurosci. 7, 85–91.
Kothur, K., Wienholt, L., Brilot, F., Dale, R.C., 2016. CSF cytokines/chemokines as biomarkers in neuroinflammatory CNS disorders: a systematic review. Cytokine 77, 227–237.
Kummerfeld, M., Meens, J., Haas, L., Baumgartner, W., Beineke, A., 2009. Generation and characterization of a polyclonal antibody for the detection of Theiler's murine encephalomyelitis virus by light and electron microscopy. J. Virol. Methods 160, 185–188.
Libbey, J.E., Fujinami, R.S., 2011. Neurotropic viral infections leading to epilepsy: focus on Theiler's murine encephalomyelitis virus. Future Virol. 6, 1339–1350.
Liddelow, S.A., Guttenplan, K.A., Clarke, L.E., Bennett, F.C., Bohlen, C.J., Schirmer, L., Bennett, M.L., Munch, A.E., Chung, W.S., Peterson, T.C., Wilton, D.K., Frouin, A., Napier, B.A., Panicker, N., Kumar, M., Buckwalter, M.S., Rowitch, D.H., Dawson, V.L., Dawson, T.M., Stevens, B., Barres, B.A., 2017. Neurotoxic reactive astrocytes are induced by activated microglia. Nature 541, 481–487.
Mizuno, T., Zhang, G., Takeuchi, H., Kawanokuchi, J., Wang, J., Sonobe, Y., Jin, S., Takada, N., Komatsu, Y., Suzumura, A., 2008. Interferon-gamma directly induces neurotoxicity through a neuron specific, calcium-permeable complex of IFN-gamma receptor and AMPA GluR1 receptor. FASEB J. 22, 1797–1806.
Mohindru, M., Kang, B., Kim, B.S., 2006. Initial capsid-specific CD4(+) T cell responses protect against Theiler's murine encephalomyelitis virus-induced demyelinating disease. Eur. J. Immunol. 36, 2106–2115.
Murray, P.D., Pavelko, K.D., Leibowitz, J., Lin, X., Rodriguez, M., 1998. CD4(+) and CD8(+) T cells make discrete contributions to demyelination and neurologic disease in a viral model of multiple sclerosis. J. Virol. 72, 7320–7329.
Neumann, H., Kotter, M.R., Franklin, R.J., 2009. Debris clearance by microglia: an essential link between degeneration and regeneration. Brain 132, 288–295.
O'Shea, J.J., Gadina, M., Siegel, R., 2013. Cytokines and cytokine receptors. In: Rich, R.R., Fleisher, T.A., Shearer, W.T., Schroeder, H.W., Frew, A.J., Weyand, C.M. (Eds.), Clinical Immunology E-Book: Principles and Practice, Fourth ed. Elsevier Saunders, pp. 108–135.
Oleszak, E.L., Chang, J.R., Friedman, H., Katsetos, C.D., Platsoucas, C.D., 2004. Theiler's virus infection: a model for multiple sclerosis. Clin. Microbiol. Rev. 17, 174–207.
Polascheck, N., Bankstahl, M., Löscher, W., 2010. The COX-2 inhibitor parecoxib is neuroprotective but not antiepileptogenic in the pilocarpine model of temporal lobe epilepsy. Exp. Neurol. 224, 219–233.
Prajeeth, C.K., Beineke, A., Iskandar, C.D., Gudi, V., Herder, V., Gerhauser, I., Haist, V., Teich, R., Huehn, J., Baumgärtner, W., Stangel, M., 2014. Limited role of regulatory T cells during acute Theiler virus-induced encephalitis in resistant C57BL/6 mice. J. Neuroinflammation 11, 180.
Prinz, M., Schmidt, H., Mildner, A., Knobeloch, K.P., Hanisch, U.K., Raasch, J., Merkler, D., Detje, C., Gutcher, I., Mages, J., Lang, R., Martin, R., Gold, R., Becher, B., Bruck, W., Kalinke, U., 2008. Distinct and nonredundant in vivo functions of IFNAR on myeloid cells limit autoimmunity in the central nervous system. Immunity 28, 675–686.
Prinz, M., Priller, J., 2014. Microglia and brain macrophages in the molecular age: from origin to neuropsychiatric disease. Nat. Rev. Neurosci. 15, 300–312.
Prinz, M., Priller, J., 2017. The role of peripheral immune cells in the CNS in steady state and disease. Nat. Neurosci. 20, 136–144.
Prinz, M., Erny, D., Hagemeyer, N., 2017. Ontogeny and homeostasis of CNS myeloid cells. Nat. Immunol. 18, 385–392.
Procaccini, C., De Rosa, V., Pucino, V., Formisano, L., Matarese, G., 2015. Animal models of multiple sclerosis. Eur. J. Pharmacol. 759, 182–191.
Richards, M.H., Getts, M.T., Podojil, J.R., Jin, Y.H., Kim, B.S., Miller, S.D., 2011. Virus expanded regulatory T cells control disease severity in the Theiler's virus mouse model of MS. J. Autoimmun. 36, 142–154.
Rock, R.B., Gekker, G., Hu, S., Sheng, W.S., Cheeran, M., Lokensgard, J.R., Peterson, P.K., 2004. Role of microglia in central nervous system infections. Clin. Microbiol. Rev. 17, 942–964 table.
Rodriguez, M., Zoecklein, L.J., Howe, C.L., Pavelko, K.D., Gamez, J.D., Nakane, S., Papke, L.M., 2003. Gamma interferon is critical for neuronal viral clearance and protection in a susceptible mouse strain following early intracranial Theiler's murine encephalomyelitis virus infection. J. Virol. 77, 12252–12265.
Schetters, S.T.T., Gomez-Nicola, D., Garcia-Vallejo, J.J., Van Kooyk, Y., 2017. Neuroinflammation: Microglia and T Cells Get Ready to Tango. Front Immunol. 8, 1905.
Schmued, L.C., Stowers, C.C., Scallet, A.C., Xu, L., 2005. Fluoro-Jade C results in ultra high resolution and contrast labeling of degenerating neurons. Brain Res. 1035, 24–31.
Seitz, S., Clarke, P., Tyler, K.L., 2018. Pharmacologic depletion of microglia increases viral load in the brain and enhances mortality in murine models of flavivirus-induced encephalitis. J. Virol. 92.
Terry, R.L., Getts, D.R., Deffrasnes, C., van Vreden, C., Campbell, I.L., King, N.J., 2012. Inflammatory monocytes and the pathogenesis of viral encephalitis. J. Neuroinflammation 9, 270.
Vandesompele, J., De Preter, K., Pattyn, F., Poppe, B., Van Roy, N., De Paepe, A., Speleman, F., 2002. Accurate normalization of real-time quantitative RT-PCR data by geometric averaging of multiple internal control genes. Genome Biol. 3 RESEARCH0034.
Vezzani, A., Fujinami, R.S., White, H.S., Preux, P.M., Blümcke, I., Sander, J.W., Löscher, W., 2016. Infections, inflammation and epilepsy. Acta Neuropathol. 131, 211–234.
Waltl, I., Käufer, C., Bröer, S., Chhatbar, C., Ghita, L., Gerhauser, I., Anjum, M., Kalinke, U., Löscher, W., 2018. Macrophage depletion by liposome-encapsulated clodronate suppresses seizures but not hippocampal damage after acute viral encephalitis. Neurobiol. Dis. 110, 192–205.
Wheeler, D.L., Sariol, A., Meyerholz, D.K., Perlman, S., 2018. Microglia are required for protection against lethal coronavirus encephalitis in mice. J. Clin. Invest. 128, 931–943.